

March 1998  
 UM-P-98/15  
 RCHEP-98/04

# Energy-dependent solar neutrino flux depletion in the Exact Parity Model and implications for SNO, SuperKamiokande and BOREXINO

Raymond R. Volkas and Yvonne Y. Y. Wong

*School of Physics*

*Research Centre for High Energy Physics*

*The University of Melbourne*

*Parkville 3052 Australia*

(*r.volcas@physics.unimelb.edu.au, ywong@physics.unimelb.edu.au*)

## Abstract

Energy-dependent solar neutrino flux reduction caused by the Mikheyev–Smirnov–Wolfenstein (MSW) effect is applied to the Exact Parity Model. Several scenarios are possible, depending on the region of parameter space chosen. The interplay between intergenerational MSW transitions and vacuum “intragenerational” ordinary–mirror neutrino oscillations is discussed. Expectations for the ratio of charged to neutral current event rates at the Sudbury Neutrino Observatory (SNO) are estimated. The implications of the various scenarios for the Boron neutrino energy spectrum and BOREXINO are briefly discussed. The consequences of MSW-induced solar neutrino depletion within the Exact Parity Model differ in interesting ways from the standard  $\nu_e \leftrightarrow \nu_{\mu, \tau}$  and  $\nu_e \leftrightarrow \nu_s$  cases. The physical causes of these differences are determined.

## I. INTRODUCTION

In the Exact Parity Model (EPM) [1], parity is an exact symmetry of nature despite the  $V - A$  character of weak interactions. Exact parity symmetry is achieved by introducing parity or “mirror” partners for each of the standard model fermions, Higgs bosons and gauge bosons. In general, colour singlet and electromagnetically neutral particles in the standard sector mix with their corresponding mirror states, leading to possibly observable experimental effects.

One of the most interesting possibilities in this regard is mixing between ordinary and mirror neutrinos [2]. In part, the EPM is an explicit theory featuring three effectively sterile light neutrino flavours in addition to  $\nu_e$ ,  $\nu_\mu$  and  $\nu_\tau$ . We shall denote the mirror neutrino flavours by  $\nu'_e$ ,  $\nu'_\mu$  and  $\nu'_\tau$ , where  $\nu'_\alpha$  is the parity partner of  $\nu_\alpha$  ( $\alpha = e, \mu, \tau$ ). Exact parity invariance imposes a simple and nontrivial constraint on standard–mirror neutrino mixing: in the absence of intergenerational mixing, the mass eigenstate neutrinos must be maximal mixtures of ordinary and mirror neutrinos. This follows immediately from the requirement that parity eigenstates must also be eigenstates of the Hamiltonian when parity is an exact symmetry. The mass/parity eigenstates are given by

$$\nu_{\alpha\pm} \equiv \frac{\nu_{\alpha L} \pm (\nu'_{\alpha R})^c}{\sqrt{2}}, \quad (1)$$

where  $\nu_{\alpha\pm} \rightarrow \pm(\nu_{\alpha\pm})^c$  under a parity transformation. When intergenerational mixing is nonzero and  $CP$  violation absent, the mass eigenstates are simply linear combinations of the  $\nu_{\alpha+}$  and, separately, the  $\nu_{\alpha-}$ :

$$\begin{aligned} \nu_{i+} &= \sum_{\alpha} U_{i\alpha}^+ \nu_{\alpha+}, \\ \nu_{i-} &= \sum_{\alpha} U_{i\alpha}^- \nu_{\alpha-}, \end{aligned} \quad (2)$$

where  $i = 1, 2, 3$  and  $U_{i\alpha}^{\pm}$  are unitary mixing matrices. Exact parity symmetry forbids mixing between positive and negative parity neutrinos in the vacuum.<sup>1</sup>

The neutrino sector of the EPM is of great interest because it can explain both the solar and atmospheric neutrino anomalies [2]. The clearest case is provided by the atmospheric neutrino anomaly. (Note that we will consider the case of small intergenerational mixing in this paper, taking our cue from the almost diagonal Kobayashi–Maskawa matrix in the quark sector.) The observed anomalous value of the ratio  $R$  of  $\mu$ -like to  $e$ -like events strongly suggests that atmospheric muon neutrinos undergo *large amplitude* oscillations into another flavour. *Large amplitude oscillations imply a large mixing angle between  $\nu_\mu$  and another flavour. This is exactly what is provided for in the EPM through maximal  $\nu_\mu \leftrightarrow \nu'_\mu$  mixing.* Furthermore, the anomalous zenith angle dependence for multi-GeV  $\mu$ -like events reported by SuperKamiokande [3] provides strong independent evidence in favour of large amplitude oscillations of  $\nu_\mu$ . The totality of atmospheric neutrino data is well explained by  $\nu_\mu \leftrightarrow \nu'_\mu$  oscillations with  $\Delta m_{2+2-}^2$  in the approximate range

$$10^{-3} \lesssim \Delta m_{2+2-}^2 / eV^2 \lesssim 10^{-2}, \quad (3)$$

where  $\Delta m_{2+2-}^2$  is the squared mass difference between  $\nu_{2+}$  and  $\nu_{2-}$  [4]. Note that if we restrict the discussion to two-flavour oscillations, then the present data allows only two

---

<sup>1</sup>If the *minimal* standard model is extended by adding a mirror sector, then both neutrinos and mirror neutrinos are massless and unmixed. We do not consider this case because it is of little interest for neutrino phenomenology.

choices: the atmospheric neutrino problem is solved either by  $\nu_\mu \leftrightarrow \nu_s$  oscillations (for which the EPM provides an explicit theory) or by  $\nu_\mu \leftrightarrow \nu_\tau$  oscillations (see Refs. [4,5] for a phenomenological study). In the future, these two alternatives may be experimentally distinguished through neutral current effects [6], upward through-going and stopping muon data [7,8], and long-baseline experiments.

The solar neutrino problem also provides strong evidence in favour of the EPM neutrino sector. GALLEX [9] and SAGE [10] observe a solar  $\nu_e$  flux that is close to half of that expected from the standard solar model when neutrino oscillations are absent. A 50%  $\nu_e$  flux reduction is exactly what is expected from the EPM due to maximal  $\nu_e \leftrightarrow \nu'_e$  oscillations for the mass range

$$10^{-10} \lesssim \Delta m_{1+1-}^2 / eV^2 \lesssim 9 \times 10^{-4}, \quad (4)$$

where the upper limit is required for consistency with the CHOOZ bound [11]. The other oscillation parameters are placed within the large region of parameter space where intergenerational solar  $\nu_e$  oscillations are unimportant. GALLEX and SAGE arguably provide the most unequivocal information regarding the nature of the solar neutrino problem. There are two reasons for this: First, theoretical calculations of the expected event rates are the most robust. Second, both detectors have been calibrated with respect to a neutrino source of known intensity. Kamiokande [12], SuperKamiokande [13] and Homestake [14] also provide important information about solar neutrinos. All three of these experiments report a significant deficit of solar neutrinos, leading to a qualitatively consistent picture of solar  $\nu_e$  depletion across the five experiments (see Table I). Furthermore, because of the different energy thresholds of the experiments, a comparison of their results provides information about the energy-dependence of the solar neutrino flux depletion. Unfortunately, the precise significance of the information obtained from Kamiokande, SuperKamiokande and Homestake is less clear than for GALLEX and SAGE for the following reasons: (i) Predictions for the Boron neutrino flux vary significantly between different versions of the standard solar model, mainly because of an uncertain  $p + {}^7\text{Be} \rightarrow \gamma + {}^8\text{B}$  cross-section. The precise value of the Boron neutrino flux deficit is therefore not as well established as one would wish. (ii) The pioneering Homestake experiment is still the only experiment that is especially sensitive to the mid-energy Beryllium neutrinos. Other experiments are needed in order to confirm their result. Fortunately, BOREXINO and the Iodine experiment will probe a similar part of the spectrum in the near future. They will either confirm or disconfirm the somewhat greater flux reduction reported by Homestake.

The purpose of this paper is to study the range of possibilities for solar neutrino flux depletion provided for by the EPM, and to determine the implications of these possibilities for, in particular, the Sudbury Neutrino Observatory (SNO) [15]. SNO will play a very important role in testing the EPM because of its ability to distinguish between solar  $\nu_e \leftrightarrow \nu_{\mu,\tau}$  oscillations and  $\nu_e \leftrightarrow \nu'_\alpha$  oscillations through its sensitivity to both charged and neutral current reactions.

It is important to understand that the EPM supplies different solar neutrino outcomes in different regions of parameter space. Hitherto [2], work within the EPM has focussed on the simplest and most characteristic possibility: First, parameters are chosen so that intergenerational solar  $\nu_e$  oscillations are unimportant. Maximal  $\nu_e \leftrightarrow \nu'_e$  oscillations in

the range of Eq.(4) then lead to an *energy-independent* 50% *flux reduction* compared to no-oscillation expectations. Furthermore, since  $\nu'_e$  states are blind to the neutral current, this case leads to an expectation that SNO will measure the standard rate for charged current relative to neutral current events. This case is in many ways the most attractive possibility within the EPM, because it is extremely simple and because it most fully utilises the predictive power of the EPM: a 50% flux depletion is the direct result of maximal  $\nu_e \leftrightarrow \nu'_e$  mixing which in turn is the direct result of exact parity invariance.

However, this case does not reproduce the greater depletion of mid-energy neutrinos that is inferred from a comparison between the Homestake rate and the other measured rates. In this paper, we will explore regions of parameter space for the EPM that are different from that considered above and hitherto. There are two principal motivations for doing so. First, we want to identify those regions of parameter space that can provide a better fit to the totality of solar neutrino data than can the 50% flux reduction region. Second, since this study will necessarily involve solar  $\nu_e$  oscillations into  $\nu_\mu$ ,  $\nu'_\mu$ ,  $\nu_\tau$  and  $\nu'_\tau$  (as well as into  $\nu'_e$ ), we will provide interesting predictions for the rate of charged current to neutral current events expected at SNO. Our study will essentially be an exploration of the Mikheyev–Smirnov–Wolfenstein (MSW) effect [16–18] within the EPM.<sup>2</sup>

Before commencing the analysis we should comment that Big Bang Nucleosynthesis poses a challenge for any model of light sterile neutrinos, due to the possible excitation of excess degrees of freedom during the relevant cosmological epoch. Fortunately, and indeed remarkably, sterile neutrino models can generally meet this challenge in full through the phenomenon of lepton asymmetry generation by active–sterile or active–mirror oscillations. For a complete discussion, see Ref. [20].

The rest of this paper is structured as follows: In Sec. II we provide a semi-quantitative analysis of the implications of the SuperKamiokande measurement for the ratio of charged to neutral current event rates at SNO. Section III deals with the mathematical formulation of the MSW effect on the EPM’s underlying maximal mixing framework. We present various MSW solutions to the solar neutrino problem within in EPM in Sec. IV. In Sec. V, we discuss the implications of the solutions for the Boron neutrino energy spectrum and the Beryllium flux, and reexamine the SNO charged to neutral current event rate, now constrained by five experiments. We conclude in Sec. VI.

## II. FROM SUPERKAMIOKANDE TO SNO

The Sudbury Neutrino Observatory (SNO) will determine whether solar  $\nu_e$ ’s oscillate into the other active flavours  $\nu_\mu$  and  $\nu_\tau$  or into sterile flavours or, to some level of sensitivity, into a combination of active and sterile flavours. *The last possibility is the generic prediction of the EPM, because mirror neutrinos are sterile with respect to ordinary weak interactions.*

---

<sup>2</sup>Note that maximal  $\nu_e \leftrightarrow \nu'_e$  oscillations can provide an energy-dependent flux reduction factor that fits all of the experiments well in the “just-so” regime [19],  $\Delta m_{1+1-}^2 \sim 5 \rightarrow 8 \times 10^{-11} \text{ eV}^2$ . An experimental confirmation of an active–sterile just-so scenario would be consistent with the EPM for a tiny region of parameter space.

In this section, we will outline the various solar neutrino outcomes possible in the EPM in different regions of parameter space. Our aim in this section is to estimate the ratio of charged to neutral current event rates that SNO will measure if the EPM is the correct theory of neutrino mixing. In this “warm-up” section, we will use as little theoretical input as possible in order to not obscure, by the technical complications of the MSW effect, the important phenomenological role played by the characteristic maximal  $\nu_\alpha \leftrightarrow \nu'_\alpha$  oscillations of the EPM. Our minimal input will be: (i) that some type of MSW effect occurs (except for Case A below); (ii) that averaged maximal vacuum  $\nu_\alpha \leftrightarrow \nu'_\alpha$  oscillations occur when the oscillation length is much less than an astronomical unit; and, (iii) that SuperKamiokande has measured the correct depletion factor for Boron neutrinos. We will revisit this issue in Sec. V, armed with more detailed information about the required  $\nu_e$  survival probability. This will allow us to further constrain our estimation of the ratio of charged to neutrino current event rates expected at SNO.

### A. Case A: vacuum $\nu_e \leftrightarrow \nu'_e$ oscillations only

Case A results from the parameter space region discussed in the Introduction and in previous papers [2]. Parameters are chosen so that the only oscillation mode important for solar neutrinos is  $\nu_e \leftrightarrow \nu'_e$  with the oscillation length set by Eq.(4). If this case is correct, SNO will measure the standard value for the ratio of charged current to neutral current events. They should also, of course, confirm the substantial depletion of Boron neutrinos reported by Kamiokande and SuperKamiokande.

### B. Cases employing the MSW effect

Suppose intergenerational solar  $\nu_e$  oscillations are now switched on by choosing a different point in parameter space. In order to obtain substantial intergenerational oscillations while simultaneously keeping the relevant mixing angles small, the MSW mechanism must be invoked. We will discuss the details of MSW transitions within the EPM in Sec. III. For the purposes of this section, we will merely suppose that MSW transitions exist and deplete solar neutrinos in an appropriate energy-dependent fashion.

The interesting issue for SNO is the flavour content of the solar neutrino flux at the Earth. In general, MSW transitions will process some of the solar  $\nu_e$  flux into second and third generation neutrinos and mirror neutrinos in the interior of the sun such that

$$\phi_0^\odot(e, E) = \phi^\odot(e, E) + \phi^\odot(e', E) + \phi^\odot(\mu, E) + \phi^\odot(\mu', E) + \phi^\odot(\tau, E) + \phi^\odot(\tau', E), \quad (5)$$

where  $\phi_0^\odot(e, E)$  is the no-oscillation standard solar model flux of  $\nu_e$  of energy  $E$  at the surface of the sun, while  $\phi^\odot(\alpha, E)$  and  $\phi^\odot(\alpha', E)$  are the fluxes of  $\nu_\alpha$  and  $\nu'_\alpha$ , respectively, at the surface of the sun. The equality in Eq.(5) follows from flux conservation. The various fluxes on the right hand side of Eq.(5) are given by

$$\phi^\odot(a, E) = P_{ea}^\odot(E) \phi_0^\odot(e, E), \quad (6)$$

where  $P_{ea}^\odot(E)$  is the matter-affected oscillation probability at the surface of the sun for  $\nu_e \leftrightarrow \nu_a$  ( $a = \alpha, \alpha'$ ). Probability conservation requires that

$$1 = P_{ee}^\odot(E) + P_{ee'}^\odot(E) + P_{e\mu}^\odot(E) + P_{e\mu'}^\odot(E) + P_{e\tau}^\odot(E) + P_{e\tau'}^\odot(E) \quad (7)$$

for each value of  $E$ .

The crucial point can now be made: *between the sun and the Earth, additional large amplitude vacuum oscillations will in general occur between the maximally mixed standard plus mirror pairs.* Vacuum intergenerational oscillations will be small given our assumption of small intergenerational mixing. Provided that the oscillation lengths for  $\nu_\alpha \leftrightarrow \nu'_\alpha$  are smaller than an astronomical unit (i.e., where the corresponding squared mass difference is  $\gtrsim 10^{-10} \text{ eV}^2$ ), maximal vacuum oscillations will induce

$$\phi^\oplus(\alpha, E) = \phi^\oplus(\alpha', E) = \frac{\phi^\odot(\alpha, E) + \phi^\odot(\alpha', E)}{2\zeta}, \quad (8)$$

where  $\phi^\oplus$  denotes the flux *at the Earth*, and  $\zeta$  is a geometric factor due to the inverse square law. This is expressed in terms of oscillation probabilities as

$$P_{e\alpha}^\oplus(E) = P_{e\alpha'}^\oplus(E) = \frac{P_{e\alpha}^\odot(E) + P_{e\alpha'}^\odot(E)}{2}, \quad (9)$$

where the superscript  $\oplus$  denotes oscillation probabilities at the Earth. The different possibilities for SNO now correspond to different oscillation length regimes for  $\nu_\alpha \leftrightarrow \nu'_\alpha$ .

Because strong evidence now exists for an atmospheric neutrino anomaly, we choose  $\Delta m_{2+2-}^2$  in the range of Eq.(3). This means that Eqs.(8) and (9) certainly hold for  $\alpha = \mu$ . The different cases discussed below correspond to the four generic possibilities for  $\Delta m_{1+1-}^2$  and  $\Delta m_{3+3-}^2$ .

### 1. Case B

Case B corresponds to the parameter choice

$$\Delta m_{1+1-}^2, \Delta m_{3+3-}^2 \gtrsim 10^{-10} \text{ eV}^2, \quad (10)$$

so that Eqs.(8) and (9) hold for  $\alpha = e, \tau$  as well as for  $\alpha = \mu$ . Combining Eqs.(5), (8) and (10) we see that the total flux of active neutrinos at the Earth will be

$$\phi^\oplus(\text{active}, E) = \frac{\phi_0^\oplus(e, E)}{2} = \frac{\phi_0^\odot(e, E)}{2\zeta}, \quad (11)$$

that is, exactly half of the no-oscillation  $\nu_e$  flux. This 50% flux reduction is a direct result of the maximal mixing constraint following from exact parity symmetry. This prediction implies that the SNO neutral current rate will be 50% of the no-oscillation expectation.

To quantify expectations for SNO, we consider the rates for charged current and neutral current events given, respectively, by

$$\begin{aligned}\Gamma_{CC} &= \int_{E_0}^{\infty} P_{ee}^{\oplus}(E) \phi_0^{\oplus}(e, E) \sigma_{CC}(E) dE, \\ \Gamma_{NC} &= \int_{E_0}^{\infty} [P_{ee}^{\oplus}(E) + P_{e\mu}^{\oplus}(E) + P_{e\tau}^{\oplus}(E)] \phi_0^{\oplus}(e, E) \sigma_{NC}(E) dE,\end{aligned}\quad (12)$$

where  $E_0$  is the energy threshold for SNO and  $\sigma_{CC}(E)$  [ $\sigma_{NC}(E)$ ] is the charged [neutral] current cross-section.

According to Eqs.(7), (9), (10) and (12), we see that the charged to neutral current rate divided by the no-oscillation expectation is given by

$$r_d \equiv \frac{(\Gamma_{CC}/\Gamma_{NC})|_{osc}}{(\Gamma_{CC}/\Gamma_{NC})|_0} = 2 \frac{\Gamma_{CC}|_{osc}}{\Gamma_{CC}|_0}, \quad (13)$$

where the characteristic factor of two is just another way of expressing the 50% flux reduction of the sum of active flavours. SNO will measure  $\Gamma_{CC}|_{osc}$ , while  $\Gamma_{CC}|_0$  depends on Boron neutrino flux predictions from the standard solar model.

Equation (13) is an exact result. In order to obtain a precise prediction for  $r_d$ , the energy-dependent survival probability must be known. However, a good estimation for  $r_d$  can be obtained from the measured Boron neutrino flux at SuperKamiokande, because the energy threshold of SNO is similar to that of SuperKamiokande. The charged current event rate at SNO relative to the no-oscillation expectation should be approximately equal to the analogous quantity measured by SuperKamiokande. In order to use the SuperKamiokande measurement of  $\Omega_{SK}$ , where

$$\Omega_{SK} \equiv \frac{\text{observed event rate}}{\text{no-oscillation event rate}}, \quad (14)$$

we have to correct for the small contribution that neutral current induced  $\nu_{\mu,\tau}e$  scattering makes to it. Using Eqs.(11) and (13) together with the relation  $\sigma^{SK}(\nu_{\mu,\tau}e) \simeq \frac{1}{6}\sigma^{SK}(\nu_e e)$  between the relevant cross-sections at SuperKamiokande, we obtain

$$r_d \sim \frac{12\Omega_{SK} - 1}{5} \quad (15)$$

for Case B. Using the information in Table I, and taking a  $2\sigma$  limit that incorporates both experimental and theoretical uncertainties, we get that

$$\Omega_{SK} \sim 0.25 \rightarrow 0.5. \quad (16)$$

The large range displayed here is mainly due to the significant theoretical uncertainty in the Boron neutrino flux. [Note also that we have focussed on SSM-BP (1995) only [21]. Other SSM calculations yield significantly different Boron neutrino fluxes [22].] Using Eq.(16), we get

$$r_d \sim 0.4 \rightarrow 1. \quad (17)$$

Note that for the upper extreme, where the Boron neutrino depletion is entirely due to averaged maximal  $\nu_e \leftrightarrow \nu'_e$  oscillations, Case B becomes identical to Case A for Boron neutrinos.

By way of comparison, the standard  $\nu_e \leftrightarrow \nu_{\mu, \tau}$  expectation is

$$r_d \sim \frac{6\Omega_{SK} - 1}{5} \sim 0.1 \rightarrow 0.4. \quad (18)$$

(Note that SuperKamiokande data only have been used to obtain this estimate. Tighter predictions are obtained when a survival probability consistent with all five solar neutrino experiments is used.) So, we see that the Case B range for  $r_d$  covers all of the values between the ranges for the standard  $\nu_e \leftrightarrow \nu_{\mu, \tau}$  and  $\nu_e \leftrightarrow \nu_s$  solutions. A clear distinction between these three possibilities therefore seems to be provided for by  $r_d$ , unless by bad luck the measured value turns out to be close to either 0.4 or 1.

## 2. Case C

Case C is defined by the parameter choice

$$\Delta m_{1+1-}^2 \lesssim 10^{-11} \text{ eV}^2, \quad \Delta m_{3+3-}^2 \gtrsim 10^{-10} \text{ eV}^2, \quad (19)$$

so that vacuum  $\nu_e \leftrightarrow \nu'_e$  oscillations do not occur. In addition, both direct transitions of  $\nu_e$  to  $\nu'_e$ , and indirect transitions via the second and third generation flavours, are negligible within the sun. We can therefore set

$$P_{ee'}^\odot(E) = 0 \quad (20)$$

to a very good level of approximation. In this case,

$$\phi^\oplus(\text{active}, E) = \frac{\phi_0^\oplus(e, E) + \phi^\oplus(e, E)}{2}. \quad (21)$$

The total flux of active flavours is larger than for Case B given the absence of vacuum  $\nu_e \leftrightarrow \nu'_e$  oscillations.

The ratio of charged to neutral current rates for this case relative to no-oscillation rates is given by

$$r_d = 2 \frac{\int_{E_0}^{\infty} P_{ee}^\oplus(E) \phi_0^\oplus(e, E) \sigma_{CC}(E) dE}{\int_{E_0}^{\infty} [1 + P_{ee}^\oplus(E)] \phi_0^\oplus(e, E) \sigma_{NC}(E) dE} \frac{\int_{E_0}^{\infty} \phi_0^\oplus(e, E) \sigma_{NC}(E) dE}{\int_{E_0}^{\infty} \phi_0^\oplus(e, E) \sigma_{CC}(E) dE}, \quad (22)$$

where an explicit expression for the energy-dependent  $\nu_e$  survival probability is required for an exact prediction. In principle, this has to be done on a case by case basis.

An approximate indication of the likely outcomes is obtained by neglecting the energy-dependence to obtain

$$r_d \sim \frac{2\langle P_{ee}^\oplus \rangle}{1 + \langle P_{ee}^\oplus \rangle}, \quad (23)$$

where  $\langle \dots \rangle$  denotes an average. Taking the SuperKamiokande measurement of  $\Omega_{SK}$ , and correcting for neutral current effects using Eq.(21), we obtain

$$\langle P_{ee}^\oplus \rangle \sim \frac{12\Omega_{SK} - 1}{11}. \quad (24)$$

For  $\Omega_{SK}$  in the range of Eq.(16), this implies that

$$r_d \sim 0.3 \rightarrow 0.6. \quad (25)$$

This case should be clearly distinguishable from Case A. It is not distinguishable from Case B or from the standard MSW  $\nu_e \rightarrow \nu_{\mu,\tau}$  scenario on the basis of  $r_d$  alone. We discuss this issue further in Secs. V and VI.

### 3. Case D

Case D corresponds to

$$\Delta m_{1+1-}^2 \gtrsim 10^{-10} \text{ eV}^2, \quad \Delta m_{3+3-}^2 \lesssim 10^{-11} \text{ eV}^2. \quad (26)$$

No especially interesting predictions can be made in this case without further information. For instance, if the MSW partners of  $\nu_e$  are  $\nu_\mu$  and  $\nu'_\mu$ , then this case reduces to Case B. If, on the other hand, the MSW partners of  $\nu_e$  are  $\nu_\tau$  and  $\nu'_\tau$ , then, in the energy-independent approximation,

$$r_d \sim \frac{\langle P_{ee}^\oplus \rangle}{\langle P_{ee}^\oplus \rangle + \langle P_{e\tau}^\oplus \rangle}. \quad (27)$$

For  $\langle P_{ee}^\oplus \rangle = 0.25$ , probability conservation at the surface of the sun requires  $0 < \langle P_{e\tau}^\oplus \rangle < 0.5$ , leading to  $r_d > 0.33$ . The lower bound on  $r_d$  increases with  $\langle P_{ee}^\oplus \rangle$ , going to 1 as  $\langle P_{ee}^\oplus \rangle$  approaches 0.5.

### 4. Case E

Finally, Case E corresponds to

$$\Delta m_{1+1-}^2, \Delta m_{3+3-}^2 \lesssim 10^{-11} \text{ eV}^2. \quad (28)$$

Again, more information is needed in this case in order to obtain predictions. If the MSW partners of  $\nu_e$  are  $\nu_\mu$  and  $\nu'_\mu$ , then this case reduces to Case C (and is also similar to the scheme analysed in Ref. [7]). If, on the other hand, the MSW partners of  $\nu_e$  are  $\nu_\tau$  and  $\nu'_\tau$ , then this case is intermediate between the standard  $\nu_e \leftrightarrow \nu_{\mu,\tau}$  and  $\nu_e \rightarrow \nu_s$  scenarios because vacuum oscillations play a negligible role.

## III. MATHEMATICAL FORMULATION OF THE MSW EFFECT IN THE EPM

The EPM predicts an energy-independent 50% reduction of the solar neutrino flux by maximal vacuum  $\nu_e \leftrightarrow \nu'_e$  oscillations that is in good quantitative agreement with experiments primarily sensitive to low-energy and to high-energy neutrinos. The significantly lower

event rate measured by Homestake, however, calls for further suppression of the mid-energy flux. Preferential energy-dependent depletion can be achieved via the MSW mechanism by restricting the relevant intergenerational squared mass difference to [17]

$$10^{-8} \lesssim \Delta m^2/eV^2 \lesssim 10^{-4}, \quad (29)$$

and [17],

$$\sin^2 2\eta \gtrsim 10^{-4}, \quad (30)$$

where  $\eta$  parameterises the mixing between the corresponding neutrino states that take part in resonant conversion.

In the following analysis, a standard neutrino mass hierarchy, i.e.,

$$m_{3\pm}^2 > m_{2\pm}^2 > m_{1\pm}^2, \quad (31)$$

is assumed such that the MSW partners of  $\nu_e$  are  $\nu_\mu$  and  $\nu'_\mu$ . Under the assumption of small intergenerational mixing, the contributions of  $\nu_\tau$  and  $\nu'_\tau$  towards the  $\nu_e$  survival probability at the Earth through vacuum oscillations is negligibly small. It then suffices to consider only the interactions between the first two generations, though the forthcoming mathematical treatments can be easily generalised to include the third generation. The remaining two-generation system thus consists of four neutrino states, where the transformation between the weak and mass/parity eigenstates is given by Eqs.(1) and (2). Explicitly,

$$\begin{pmatrix} \nu_e \\ \nu'_e \\ \nu_\mu \\ \nu'_\mu \end{pmatrix} = \frac{1}{\sqrt{2}} \begin{pmatrix} C_\phi & C_\theta & S_\phi & S_\theta \\ -C_\phi & C_\theta & -S_\phi & S_\theta \\ -S_\phi & -S_\theta & C_\phi & C_\theta \\ S_\phi & -S_\theta & -C_\phi & C_\theta \end{pmatrix} \begin{pmatrix} \nu_{1-} \\ \nu_{1+} \\ \nu_{2-} \\ \nu_{2+} \end{pmatrix}, \quad (32)$$

where  $\theta$  and  $\phi$  parameterise the two  $2 \times 2$  unitary matrices  $U_{i\alpha}^\pm$  in Eq.(2) that are responsible for the respective mixing of positive and negative parity eigenstates, and  $-\frac{\pi}{2} \leq \theta, \phi \leq \frac{\pi}{2}$ . Exact parity symmetry thereby reduces a nominally six-angle problem (if  $CP$  is conserved) to a two-angle task. (A generic  $4 \times 4$  orthogonal matrix consists of six independent parameters.)

Note that, at this stage, we do not make any assumptions regarding the signs of  $\Delta m_{1+1-}^2$  and  $\Delta m_{2+2-}^2$ , and Eq.(32) does not imply in any way that  $\nu_{1+}$  ( $\nu_{2+}$ ) is heavier than  $\nu_{1-}$  ( $\nu_{2-}$ ). This is because, firstly, we have no prior reasons for doing so. Secondly, since neutrino states of unlike parity do not mix in a gauge theoretic sense (i.e., the Lagrangian of the EPM in vacuum does not contain parity-violating terms such as  $m\bar{\nu}_{1+}\nu_{2-}$  for  $\nu_{1+} \leftrightarrow \nu_{2-}$  [2]), we would expect the *effective* mixing of like-parity (such as  $\nu_{1+} \leftrightarrow \nu_{2+}$ ) and of unlike-parity eigenstates to experience different forms of matter enhancement. Ours being a two-angle problem renders the quantification of this difference a relatively simple task. Henceforth, we shall denote the heavier (lighter) of  $\nu_{1\pm}$  and of  $\nu_{2\pm}$  as  $\nu_{1h}$  and  $\nu_{2h}$  ( $\nu_{1\ell}$  and  $\nu_{2\ell}$ ) such that

$$\begin{pmatrix} \nu_e \\ \nu'_e \\ \nu_\mu \\ \nu'_\mu \end{pmatrix} = U \begin{pmatrix} \nu_{1\ell} \\ \nu_{1h} \\ \nu_{2\ell} \\ \nu_{2h} \end{pmatrix} = \begin{pmatrix} U_{e1\ell} & U_{e1h} & U_{e2\ell} & U_{e2h} \\ U_{e'1\ell} & U_{e'1h} & U_{e'2\ell} & U_{e'2h} \\ U_{\mu 1\ell} & U_{\mu 1h} & U_{\mu 2\ell} & U_{\mu 2h} \\ U_{\mu'1\ell} & U_{\mu'1h} & U_{\mu'2\ell} & U_{\mu'2h} \end{pmatrix} \begin{pmatrix} \nu_{1\ell} \\ \nu_{1h} \\ \nu_{2\ell} \\ \nu_{2h} \end{pmatrix}, \quad (33)$$

in order to keep the analysis as general as possible.

The problem now becomes one of solving the Schrödinger equation [23]:

$$\begin{aligned} i \frac{d}{dx} \begin{pmatrix} \nu_e \\ \nu'_e \\ \nu_\mu \\ \nu'_\mu \end{pmatrix} &= \mathcal{H} \begin{pmatrix} \nu_e \\ \nu'_e \\ \nu_\mu \\ \nu'_\mu \end{pmatrix} = \frac{1}{2E} (U \mathcal{M} U^{-1} + \mathcal{H}_{int}) \begin{pmatrix} \nu_e \\ \nu'_e \\ \nu_\mu \\ \nu'_\mu \end{pmatrix} \\ &= \frac{1}{2E} \left[ U \begin{pmatrix} m_{1\ell}^2 & 0 & 0 & 0 \\ 0 & m_{1h}^2 & 0 & 0 \\ 0 & 0 & m_{2\ell}^2 & 0 \\ 0 & 0 & 0 & m_{2h}^2 \end{pmatrix} U^{-1} + \begin{pmatrix} A_e & 0 & 0 & 0 \\ 0 & 0 & 0 & 0 \\ 0 & 0 & A_\mu & 0 \\ 0 & 0 & 0 & 0 \end{pmatrix} \right] \begin{pmatrix} \nu_e \\ \nu'_e \\ \nu_\mu \\ \nu'_\mu \end{pmatrix}, \end{aligned} \quad (34)$$

where  $U$  is the mixing matrix in Eq.(33),  $E$  is the neutrino energy, and  $m_{1\ell}^2$ ,  $m_{1h}^2$ ,  $m_{2\ell}^2$  and  $m_{2h}^2$  are the squared masses of the mass/parity eigenstates  $\nu_{1\ell}$ ,  $\nu_{1h}$ ,  $\nu_{2\ell}$  and  $\nu_{2h}$  respectively. The interaction terms for  $\nu_e$  and  $\nu_\mu$  ( $\nu'_e$  and  $\nu'_\mu$  are inert) are

$$\begin{aligned} A_e &= A_{CC} + A_{NC}, \\ A_\mu &= A_{NC}, \end{aligned} \quad (35)$$

where  $CC$  stands for charged current,  $NC$  for neutral current and

$$\begin{aligned} A_{CC} &= 2\sqrt{2}G_F E N_e(x), \\ A_{NC} &= -\sqrt{2}G_F E N_n(x), \end{aligned} \quad (36)$$

where  $G_F$  is the Fermi constant,  $N_e(x)$  the electron number density at position  $x$  in the neutrino's path, and  $N_n(x)$  the neutron number density. If  $U^m$  is a density-dependent unitary transformation that puts the total Hamiltonian  $\mathcal{H}$  in an instantaneous mass basis  $\nu_i^m$  such that

$$\nu_\alpha = \sum_i U_{\alpha i}^m \nu_i^m, \quad \alpha = e, e', \mu, \mu', \quad i = 1\ell, 1h, 2\ell, 2h, \quad (37)$$

the Schrödinger equation in Eq.(34) can be rewritten as:

$$\begin{aligned} i \frac{d}{dx} \begin{pmatrix} \nu_{1\ell}^m \\ \nu_{1h}^m \\ \nu_{2\ell}^m \\ \nu_{2h}^m \end{pmatrix} &= \mathcal{H}^m \begin{pmatrix} \nu_{1\ell}^m \\ \nu_{1h}^m \\ \nu_{2\ell}^m \\ \nu_{2h}^m \end{pmatrix} = U^{m-1} (\mathcal{H} - i \frac{d}{dx}) U^m \begin{pmatrix} \nu_{1\ell}^m \\ \nu_{1h}^m \\ \nu_{2\ell}^m \\ \nu_{2h}^m \end{pmatrix} \\ &= \left[ \frac{1}{2E} \begin{pmatrix} m_{1\ell}^2(x) & 0 & 0 & 0 \\ 0 & m_{1h}^2(x) & 0 & 0 \\ 0 & 0 & m_{2\ell}^2(x) & 0 \\ 0 & 0 & 0 & m_{2h}^2(x) \end{pmatrix} - U^{m-1} i \frac{d}{dx} U^m \right] \begin{pmatrix} \nu_{1\ell}^m \\ \nu_{1h}^m \\ \nu_{2\ell}^m \\ \nu_{2h}^m \end{pmatrix}, \end{aligned} \quad (38)$$

where  $m_{1\ell}^2(x)$ ,  $m_{1h}^2(x)$ ,  $m_{2\ell}^2(x)$  and  $m_{2h}^2(x)$  are the squared mass eigenvalues of the instantaneous mass eigenstates  $\nu_{1\ell}^m$ ,  $\nu_{1h}^m$ ,  $\nu_{2\ell}^m$  and  $\nu_{2h}^m$  respectively. Given the initial conditions

$$\nu_e(x_i) = 1, \quad \nu'_e(x_i) = \nu_\mu(x_i) = \nu'_\mu(x_i) = 0, \quad (39)$$

where  $x_i$  is the  $\nu_e$  production position, the probability that a  $\nu_e$  produced in the sun will be detected on Earth is expressed as

$$P_{ee}^{\oplus}(E) = \left| \sum_{i,j} U_{ei}^m(x_i) \exp \left[ -i \int_{x_i}^{x_f} \mathcal{H}_{ij}^m dx \right] U_{ej} \right|^2, \quad (40)$$

where  $i, j = 1\ell, 1h, 2\ell, 2h$ , the exponential of the integral from  $x_i$  to the detection position  $x_f$  is the solution to Eq.(38),  $U^m(x_i)$  is the density-dependent mixing matrix at the point of  $\nu_e$  production and we have chosen  $U$  real (assuming that  $CP$  is conserved). The term  $\exp \left[ -i \int_{x_i}^{x_f} \mathcal{H}_{ij}^m dx \right]$  represents the amplitude of a transition from  $\nu_i^m$  to  $\nu_j^m$  and vice versa.

For future reference, note that for a  $2\nu$  system, after phase-averaging, the  $\nu_e$  survival probability is given by [24]

$$P_{ee}^{\oplus}(E)|_{2\nu} = \frac{1}{2} + \left( \frac{1}{2} - P_R \right) \cos 2\eta_m(x_i) \cos 2\eta \equiv P_{2\nu MSW}, \quad (41)$$

where  $\eta$  is the vacuum mixing angle,  $\eta_m(x_i)$  the matter mixing angle at the  $\nu_e$  production position, and  $P_R$  the level-crossing probability evaluated at resonance. [A common practice is to multiply the  $P_R$  term by a step function,  $\theta(E - E_A)$ , where  $E_A$  is the minimum energy a neutrino produced at  $x_i$  must possess for a resonance to take place inside the sun [25]. It shall be omitted for the convenience of typesetting.] We shall refer to this  $2\nu$  survival probability as the MSW transition probability  $P_{2\nu MSW}$ . Bearing in mind that the same expression can be obtained by considering probabilities instead of amplitudes, we shall adopt the same classical attitude for the rest of the analysis.

An analysis involving two effectively sterile neutrinos approximately maximally mixed with  $\nu_e$  and  $\nu_\mu$  respectively was carried out in Ref. [26]. The “intragenerational” mass differences were assumed to be much smaller than the intergenerational mass difference, the latter of which was responsible for a  $\nu_e \leftrightarrow \nu_\mu$  MSW resonance. Our case differs in that the explanation of the atmospheric neutrino anomaly by maximal vacuum  $\nu_\mu \leftrightarrow \nu'_\mu$  oscillations requires the squared mass difference between  $\nu_{2+}$  and  $\nu_{2-}$  to lie within the range of Eq.(3). These masses are much larger than the MSW masses in Eq.(29), i.e.,

$$\Delta m_{2+2-}^2 \gg \Delta m_{21}^2, \quad (42)$$

where  $\Delta m_{21}^2 = m_{2\ell}^2 - m_{1h}^2$ . On the other hand, the squared mass difference between  $\nu_{1\ell}$  and  $\nu_{1h}$  is constrained only by an experimental upper bound of  $9 \times 10^{-4} eV^2$  from Eq.(4). Thus, analytically *a priori* well-approximated MSW solutions exist for three distinct neutrino mass hierarchies, which we shall denote as Cases B1, B2, and C respectively: Case B1:  $\Delta m_{1+1-}^2, \Delta m_{2+2-}^2 \gg \Delta m_{21}^2$ ,

Case B2:  $\Delta m_{2+2-}^2 \gg \Delta m_{21}^2 \gg \Delta m_{1+1-}^2 \gtrsim 10^{-10} eV^2$ ,

Case C:  $\Delta m_{2+2-}^2 \gg \Delta m_{21}^2 \gg \Delta m_{1+1-}^2, \Delta m_{1+1-}^2 \lesssim 10^{-11} eV^2$ .

These somewhat playful labels are chosen for consistency with Sec. II, i.e., the generic predictions for SNO for Case B in Sec. II hold for both neutrino mass hierarchies defined in Cases B1 and B2, and similarly for Case C. In the following subsections, we shall derive the  $\nu_e$  survival probability for each case.

### A. Case B1

Case B1 assumes the following neutrino mass hierarchy:

$$\Delta m_{1+1-}^2, \Delta m_{2+2-}^2 \gg \Delta m_{21}^2. \quad (43)$$

In this analysis, we make one further assumption that

$$\Delta m_{1+1-}^2 \sim 10^{-3} eV^2 \quad (44)$$

for simplicity. The squared masses of the instantaneous mass eigenstates for the relevant solar densities are shown in Fig. 1.

We identify the point  $R$ , at which  $\nu_{1h}^m$  and  $\nu_{2\ell}^m$  almost cross, as an intergenerational MSW resonance. Large  $\Delta m_{1+1-}^2$  and  $\Delta m_{2+2-}^2$  (compared with  $\Delta m_{21}^2$ ) ensure that  $\nu_e \leftrightarrow \nu'_e$  and  $\nu_\mu \leftrightarrow \nu'_\mu$  oscillations remain close to maximal in its vicinity. Consequently, matter effects are most strongly felt by  $\nu_{1h}$  and  $\nu_{2\ell}$ , leading to the instantaneous mass eigenstates  $\nu_{1h}^m$  and  $\nu_{2\ell}^m$  bearing little resemblance to their vacuum counterparts. The evolution of  $\nu_{1\ell}$  and  $\nu_{2h}$  near  $R$ , on the other hand, is only slightly affected by matter, so that

$$\begin{aligned} \nu_{1\ell}^m &\simeq \nu_{1\ell}, \\ \nu_{2h}^m &\simeq \nu_{2h}. \end{aligned} \quad (45)$$

Provided Eq.(44) is satisfied, Eq.(45) will continue to hold at densities  $\rho \gg \rho_R$  in the sun. Thus, to a very good level of approximation,

$$\begin{aligned} U_{e1\ell}^m(x_i) &= U_{e1\ell}, \\ U_{e2h}^m(x_i) &= U_{e2h}, \end{aligned} \quad (46)$$

which are virtually density-independent. [Note that if  $\Delta m_{1+1-}^2$  satisfies Eq.(43) but is, at the same time, sufficiently small (say,  $\sim 10^{-5} eV^2$ ), matter effects can cause  $\nu_e$  and  $\nu'_e$  to depart from their mutual maximal mixing at  $\rho \gg \rho_R$ .  $U_{e1\ell}^m(x_i)$  becomes density-dependent and may be drastically different from its vacuum counterpart. The quantification of this effect is relatively simple. For our purposes, however, we shall not consider it here.] Thus,  $\nu_{1\ell}^m$  ( $\sim \nu_{1\ell}$ ) and  $\nu_{2h}^m$  ( $\sim \nu_{2h}$ ) decouple from the system and evolve adiabatically such that after phase-averaging, we may write, following the procedures in Ref. [27], the  $\nu_e$  survival probability as

$$\begin{aligned} P_{ee}^\oplus(E) &= |U_{e1\ell}|^4 + |U_{e2h}|^4 + \left| \sum_{i,j=1h,2\ell} U_{ei}^m(x_i) \exp \left[ -i \int_{x_i}^{x_f} \mathcal{H}_{ij}^m dx \right] U_{ej} \right|^2 \\ &= |U_{e1\ell}|^4 + |U_{e2h}|^4 + (1 - |U_{e1\ell}|^2 - |U_{e2h}|^2)^2 P_{2\nu MSW}, \end{aligned} \quad (47)$$

where

$$P_{2\nu MSW} = \left| \sum_{i,j=1h,2\ell} \frac{U_{ei}^m(x_i)}{\sqrt{U_{e1h}^m + U_{e2\ell}^m}} \exp \left[ -i \int_{x_i}^{x_f} \mathcal{H}_{ij}^m dx \right] \frac{U_{ej}}{\sqrt{U_{e1h}^2 + U_{e2\ell}^2}} \right|^2, \quad (48)$$

and  $U_{e1h}^{m2} + U_{e2\ell}^{m2} = U_{e1h}^2 + U_{e2\ell}^2$  by unitarity. The physical interpretation of Eqs.(47) and (48) follows simply. At well above the resonance density, a fraction  $|U_{e1\ell}^m(x_i)|^2$  ( $\sim |U_{e1\ell}|^2$ ) and another  $|U_{e2h}^m(x_i)|^2$  ( $\sim |U_{e2h}|^2$ ) of the  $\nu_e$ 's produced at  $x_i$  populate the instantaneous mass eigenstates  $\nu_{1\ell}^m$  ( $\sim \nu_{1\ell} \sim \frac{1}{2}$ ) and  $\nu_{2h}^m$  ( $\sim \nu_{2h} \sim 0$ ) respectively. The remaining  $(1 - |U_{e1\ell}|^2 - |U_{e2h}|^2 \sim \frac{1}{2})$  is distributed in  $\nu_{1h}^m$  and  $\nu_{2\ell}^m$  in a density-dependent ratio,  $\cos^2 2\eta_m : \sin^2 2\eta_m$ , where

$$\cos \eta_m = \frac{U_{e1h}^m}{\sqrt{U_{e1h}^{m2} + U_{e2\ell}^{m2}}}, \quad \sin \eta_m = \frac{U_{e2\ell}^m}{\sqrt{U_{e1h}^{m2} + U_{e2\ell}^{m2}}}, \quad (49)$$

and  $\eta_m \sim \frac{\pi}{2}$  for  $\rho \gg \rho_R$ . So the  $\nu_e$ 's produced in the region  $\rho \gg \rho_R$  near the centre of the sun populate  $\nu_{1\ell}^m$ ,  $\nu_{1h}^m$ ,  $\nu_{2\ell}^m$  and  $\nu_{2h}^m$  in the approximate ratio  $\frac{1}{2} : 0 \frac{1}{2} : 0$ . The half residing in  $\nu_{2\ell}^m$  participate in resonant conversion at  $R$ , while the other half in  $\nu_{1\ell}^m$  ( $\sim \nu_{1\ell}$ ) propagate adiabatically to the surface of the sun without passing through a resonance.

To study the intergenerational MSW resonance, we may treat the  $\nu_{1h} \leftrightarrow \nu_{2\ell}$  subsystem as forming two orthogonal pseudo-weak eigenstates,  $\nu_a$  and  $\nu_b$ , that convert resonantly into each other at  $R$ , i.e.,

$$\begin{pmatrix} \nu_{1\ell} \\ \nu_a \\ \nu_b \\ \nu_{2h} \end{pmatrix} = \mathcal{R}(\eta) \begin{pmatrix} \nu_{1\ell} \\ \nu_{1h} \\ \nu_{2\ell} \\ \nu_{2h} \end{pmatrix} = \begin{pmatrix} 1 & 0 & 0 & 0 \\ 0 & \cos \eta & \sin \eta & 0 \\ 0 & -\sin \eta & \cos \eta & 0 \\ 0 & 0 & 0 & 1 \end{pmatrix} \begin{pmatrix} \nu_{1\ell} \\ \nu_{1h} \\ \nu_{2\ell} \\ \nu_{2h} \end{pmatrix}, \quad (50)$$

where

$$\cos \eta = \frac{U_{e1h}}{\sqrt{U_{e1h}^2 + U_{e2\ell}^2}}, \quad \sin \eta = \frac{U_{e2\ell}}{\sqrt{U_{e1h}^2 + U_{e2\ell}^2}}, \quad (51)$$

are the vacuum counterparts of the parameters in Eq.(49). With this parameterisation, we may rewrite the mixing matrix  $U$  as

$$U = \mathcal{T}(\text{others}) \mathcal{R}(\eta), \quad (52)$$

where  $\mathcal{T}(\text{others})$  is a unitary matrix responsible for other mixing modes. Since  $\nu_{1h} \leftrightarrow \nu_{2\ell}$  is the only matter-enhanced mixing mode, with the matter mixing angle  $\eta_m$  taking on the maximal value  $\frac{\pi}{4}$  at resonance, we may approximate  $U^m$  as

$$\begin{aligned} U^m &= \mathcal{T}(\text{others}) \mathcal{R}(\eta_m) \\ &= U \mathcal{R}^{-1}(\eta) \mathcal{R}(\eta_m), \end{aligned} \quad (53)$$

in the same manner that is adopted in the study of  $3\nu$  schemes [25,28]. Equation (53) then allows us to recast the integrand  $\mathcal{H}_{ij}^m$  in Eq.(48) into

$$\begin{aligned} \mathcal{H}^m &= U^{m-1} (\mathcal{H} - i \frac{d}{dx}) U^m \\ &= \mathcal{R}^{-1}(\eta_m) (\mathcal{H}_{\text{eff}} - i \frac{d}{dx}) \mathcal{R}(\eta_m), \end{aligned} \quad (54)$$

where

$$\begin{aligned}\mathcal{H}_{eff} &= \mathcal{R}(\eta)U^{-1}\mathcal{H}U\mathcal{R}^{-1}(\eta) \\ &= \frac{1}{2E}[\mathcal{R}(\eta)\mathcal{M}\mathcal{R}^{-1}(\eta) + \mathcal{R}(\eta)U^{-1}\mathcal{H}_{int}U\mathcal{R}^{-1}(\eta)],\end{aligned}\quad (55)$$

by Eqs.(34) and (38). The  $2 \times 2$  submatrix  $\mathcal{H}_{effij}$ , where  $i, j = 1h, 2\ell$  (i.e., the  $2 - 3$  sector of  $\mathcal{H}_{eff}$ ), is thus the effective Hamiltonian that governs the evolution of the pseudo-weak eigenstates  $\nu_a$  and  $\nu_b$ . Subtracting a common phase,  $\mathcal{H}_{effij}$  takes on the form

$$\mathcal{H}_{effij} \doteq \frac{1}{4E} \begin{pmatrix} -\Delta m_{21}^2 \cos 2\eta + A_{eff} & \Delta m_{21}^2 \sin 2\eta + A_{ind} \\ \Delta m_{21}^2 \sin 2\eta + A_{ind} & \Delta m_{21}^2 \cos 2\eta - A_{eff} \end{pmatrix}, \quad (56)$$

where  $A_{eff}$ , the effective density, is

$$\begin{aligned}A_{eff} &= A_{CC}(U_{e1h}^2 + U_{e2\ell}^2) \\ &+ A_{NC}[\cos 2\eta(U_{e1h}^2 - U_{e2\ell}^2 + U_{\mu1h}^2 - U_{\mu2\ell}^2) + 2 \sin 2\eta(U_{e1h}U_{e2\ell} + U_{\mu1h}U_{\mu2\ell})],\end{aligned}\quad (57)$$

and

$$A_{ind} = A_{NC}[2 \cos 2\eta(U_{e1h}U_{e2\ell} + U_{\mu1h}U_{\mu2\ell}) - \sin 2\eta(U_{e1h}^2 - U_{e2\ell}^2 + U_{\mu1h}^2 - U_{\mu2\ell}^2)], \quad (58)$$

where the subscript *ind* stands for induced. The physical significance of this term will be discussed in due course. The quantities  $A_{eff}$  and  $A_{ind}$  evaluated for various combinations of  $\nu_{1h}$  and  $\nu_{2\ell}$  in the EPM are shown in Table II. The effective Hamiltonian  $\mathcal{H}_{effij}$  is analogous to that for a standard  $2\nu$  system. The solution to

$$i \frac{d}{dx} \begin{pmatrix} \nu_a \\ \nu_b \end{pmatrix} = \mathcal{H}_{effij} \begin{pmatrix} \nu_a \\ \nu_b \end{pmatrix} \quad (59)$$

will thus give us the term  $P_{2\nu MSW}$  that is equivalent to the MSW transition probability given by Eq.(41), with a squared mass difference of  $\Delta m_{21}^2$  and mixing angle  $\eta$  defined in Eq.(51) in a medium of effective density  $A_{eff}$  given by Eq.(57) (plus some non-standard features to be discussed).

We now look at the  $2\nu$  subsystem more closely. In general, the effective density  $A_{eff}$  in Eq.(57) contains both charged and neutral current interaction terms, though the latter's contribution is negligible if intergenerational mixing is small, i.e.,

$$A_{eff} \approx \frac{1}{2}A_{CC}, \quad (60)$$

for  $|U_{e1h}|, |U_{\mu2\ell}| \sim \frac{1}{\sqrt{2}}$  and  $|U_{e2\ell}|, |U_{\mu1h}| \sim 0$ . Equation (60), in turn, supports an approximate resonance condition given by

$$A_{CC} \approx 2\Delta m_{21}^2 \cos 2\eta, \quad (61)$$

which may be rearranged into a more illuminating form:

$$E_A \approx \frac{\Delta m_{21}^2 \cos 2\eta}{\sqrt{2} G_F N_e(x_i)}, \quad (62)$$

where the subscript  $A$  stands for adiabatic and  $N_e(x_i)$  is the electron number density at the  $\nu_e$  production position. The quantity  $E_A$  determines the location of the adiabatic edge of the MSW transition probability in the limit of small intergenerational mixing, such that for all neutrinos produced at  $x_i$ , only the ones with energy  $E > E_A$  will be resonantly converted into other species. Comparing Eq.(62) to its counterpart in the standard  $\nu_e \leftrightarrow \nu_{\mu, \tau}$  scenario (where  $A_{eff} = A_{CC}$ ), our naturally smaller effective density automatically puts the adiabatic edge at twice the energy of the latter for a given  $\Delta m_{21}^2$  and  $\eta$ . Equations (60), (61) and (62) are exact and *independent* of intergenerational mixing (provided it is nonzero), according to Table II if (i)  $\nu_{1h}$  and  $\nu_{2\ell}$  are both positive or both negative parity eigenstates, or (ii)  $\theta = \phi$  for all possible combinations of  $\nu_{1h}$  and  $\nu_{2\ell}$ . Nonetheless, while we are not considering large  $\theta$  and  $\phi$  cases, Eq.(62) will locate the adiabatic edge with sufficient accuracy regardless of the exact identities of  $\nu_{1h}$  and  $\nu_{2\ell}$  for the present analysis in the limit of small intergenerational mixing. Taking  $|U_{e1\ell}| \sim \frac{1}{\sqrt{2}}$  and  $|U_{e2h}| \sim 0$ , the  $\nu_e$  survival probability for Case B1 in Eq.(47) is well approximated by

$$P_{ee}^{\oplus}(E) \approx \frac{1}{4} + \frac{1}{4} P_{2\nu MSW}. \quad (63)$$

Equation (63) is plotted in Fig. 2, juxtaposed with the respective survival probabilities for the standard  $\nu_e \leftrightarrow \nu_{\mu, \tau}$  and  $\nu_e \leftrightarrow \nu_s$  cases evaluated for the same oscillation parameters for comparison.

The second non-standard feature is the presence of density-dependent terms,  $A_{ind}$ , in the off-diagonal elements of the effective Hamiltonian in Eq.(56), representing some form of matter-induced mixing similar to that discussed in Ref. [7]. This matter-induced mixing manifests itself primarily in the non-adiabatic high-energy end of the MSW transition probability. Explicitly, if we write the effective Hamiltonian as

$$\mathcal{H}_{eff} = \begin{pmatrix} -\xi(x) & \kappa(x) \\ \kappa(x) & \xi(x) \end{pmatrix}, \quad (64)$$

assuming a linear density profile, the level-crossing probability may be written as [29,30]

$$P_R = \exp \left[ -\frac{\pi}{2} \gamma_R \right], \quad (65)$$

where the adiabaticity parameter  $\gamma_R$  is

$$\gamma_R = 2 \frac{\kappa^2(x)}{\left| \frac{d\xi(x)}{dx} \right|} \bigg|_{x=x_R}, \quad (66)$$

evaluated at resonance;  $P_R$ 's dependence on the matter-induced mixing term  $A_{ind}$  is obvious.

In the context of the EPM, the extent to which matter-induced mixing affects the non-adiabatic conversion of solar neutrinos depends largely on the identities of  $\nu_{1h}$  and  $\nu_{2\ell}$ . In particular, the mixing of like-parity and of unlike-parity eigenstates receive considerably

different forms of matter enhancement. With reference to Table II, if  $\nu_{1h}$  and  $\nu_{2\ell}$  are like-parity eigenstates,  $A_{ind}$  vanishes exactly, leaving behind in Eq.(56) the standard vacuum parameters  $\Delta m_{21}^2$  and  $\eta$ , where  $\eta$  is now replaced with  $\theta$  or  $\phi$  for  $\nu_{1+} \leftrightarrow \nu_{2+}$  and  $\nu_{1-} \leftrightarrow \nu_{2-}$  respectively. Thus, parity-conserving, direct mixing modes are enhanced naturally by matter effects in a familiar resonant fashion. In addition, the resonant enhancement of one mixing mode is completely independent of the other, that is, if the resonant mode is  $\nu_{1+} \leftrightarrow \nu_{2+}$  where  $\theta$  is the mixing angle responsible,  $\phi$  does not enter the scene.

In the EPM, the *apparent* mixing of unlike-parity eigenstates in vacuum is an observational effect due to mixing through other parity-conserving channels. In matter, *apparent* parity-violating mixing is, to some extent, conjured up by matter, as suggested by the general presence of an  $A_{ind}$  term for the matter-enhanced effective mixing of  $\nu_{1-} \leftrightarrow \nu_{2+}$  and  $\nu_{1+} \leftrightarrow \nu_{2-}$  respectively. Furthermore, the strength of this matter-induced mixing is dependent on the relative amplitude of the  $\theta$  and  $\phi$  modes. An inspection of Table II reveals that, depending on the sign of  $\sin(\theta - \phi)$ , matter-induced mixing may enhance or suppress the non-adiabatic conversion of  $\nu_e$  by decreasing or increasing respectively the matter oscillation length at resonance. The magnitude of this matter-induced mixing is, in part, controlled by the neutron density at resonance but is most severe when  $\theta$  and  $\phi$  differ significantly. Consider the case of effective  $\nu_{1-} \leftrightarrow \nu_{2+}$  mixing. The contribution from matter-induced mixing relative to vacuum mixing is represented by the ratio

$$\Lambda = \left| \frac{A_{NC} \cos 2\eta \sin(\theta - \phi)}{\Delta m_{21}^2 \sin 2\eta} \right|_{x=x_R}, \quad (67)$$

evaluated at resonance. Using the resonance condition in Eq.(61), we find that

$$\Lambda \cong \frac{N_n(x_R)}{N_e(x_R)} \left| \frac{\cos^2 2\eta \sin(\theta - \phi)}{\sin 2\eta} \right| \cong \frac{1}{2} \frac{N_n(x_R)}{N_e(x_R)} \left| 1 - \frac{\tan \phi}{\tan \theta} \right|, \quad (68)$$

by various relations in Table II to first order in  $\sin \eta$ . Matter-induced and vacuum mixing are comparable if  $\Lambda \approx 1$ . Given that the electron number density is some two to six times the neutron number density in the interior of the sun [21], this corresponds to

$$\frac{\tan \phi}{\tan \theta} < 2 \frac{N_e(x_R)}{N_n(x_R)} + 1 = 5 \rightarrow 13, \quad (69)$$

if  $\theta$  and  $\phi$  are in the same quadrant, or

$$\frac{\tan \phi}{\tan \theta} < 1 - 2 \frac{N_e(x_R)}{N_n(x_R)} = -11 \rightarrow -3, \quad (70)$$

if  $\theta$  and  $\phi$  are in different quadrants, in order for matter-induced mixing to be recessive. The most extreme scenario is when the  $\theta$  mode is completely absent, such that  $\sin \eta = 0$  and matter-induced mixing completely dominates. The consequential shift of the adiabatic edge in the MSW transition probability is negligible. On the non-adiabatic side, assuming a linear density profile, the level-crossing probability is determined by

$$\begin{aligned}
P_R &= \exp \left[ -\frac{\pi}{4} \frac{\Delta m_{21}^2}{E} \frac{\left( \frac{|A_{NC}|}{\Delta m_{21}^2} \sin \phi \right)^2}{\left| \frac{1}{A_{eff}} \frac{dA_{eff}}{dx} \right|} \right] \Big|_{x=x_R} \\
&= \exp \left[ -\frac{\pi}{4} \frac{\Delta m_{21}^2}{E} \frac{\sin^2 2\phi}{\left| \frac{1}{A_{eff}} \frac{dA_{eff}}{dx} \right|} \left( \frac{|A_{NC}|}{2\Delta m_{21}^2 \cos \phi} \right)^2 \right] \Big|_{x=x_R}.
\end{aligned} \tag{71}$$

Comparing this with its counterpart in the case where  $\theta = \phi \equiv \varphi$  (such that  $A_{ind}$  vanishes exactly, see Table II), that is,

$$P_R = \exp \left[ -\frac{\pi}{4} \frac{\Delta m_{21}^2}{E} \frac{\sin^2 2\varphi}{\cos 2\varphi} \frac{1}{\left| \frac{1}{A_{eff}} \frac{dA_{eff}}{dx} \right|} \right] \Big|_{x=x_R}, \tag{72}$$

we observe that approximate agreement between Eqs.(71) and (72) in the small intergenerational mixing limit requires (for the same  $\Delta m_{21}^2$ ),

$$\begin{aligned}
\sin^2 2\phi &\cong \left( \frac{2\Delta m_{21}^2}{|A_{NC}|} \right)^2 \sin^2 2\varphi \cong \left( \frac{2N_e(x_R)}{N_n(x_R)} \right)^2 \sin^2 2\varphi \\
&\cong (16 \rightarrow 144) \sin^2 2\varphi.
\end{aligned} \tag{73}$$

Thus, if we fit the  $\nu_e$  survival probability in Eq.(63) to experimental data for the  $\theta = \phi$  case (so that the identities of  $\nu_{1h}$  and  $\nu_{2\ell}$  do not matter), we know automatically from Eqs.(60) to (62) that approximately the same  $\Delta m_{21}^2$  will account for  $\nu_{1-} \leftrightarrow \nu_{2+}$  with  $\theta = 0$ , while the mixing required,  $\sin^2 2\phi$ , is some 16 to 144 times that for  $\theta = \phi$ , under the assumption of small intergenerational mixing according to Eq.(73).

On the other hand, if  $\phi$  is set to zero and  $\theta$  allowed to vary for  $\nu_{1-} \leftrightarrow \nu_{2+}$ , we see from Table II that both vacuum and matter-induced mixing contribute to the level-crossing probability, i.e.,

$$\begin{aligned}
P_R &= \exp \left[ -\frac{\pi}{4} \frac{\Delta m_{21}^2}{E} \frac{\left( \sin 2\eta + \frac{A_{NC}}{\Delta m_{21}^2} \cos 2\eta \sin \theta \right)^2}{\cos 2\eta} \frac{1}{\left| \frac{1}{A_{eff}} \frac{dA_{eff}}{dx} \right|} \right] \Big|_{x=x_R} \\
&= \exp \left[ -\frac{\pi}{4} \frac{\Delta m_{21}^2}{E} \frac{\sin^2 2\theta}{\left| \frac{1}{A_{eff}} \frac{dA_{eff}}{dx} \right|} \frac{\left( 1 - \frac{|A_{NC}|}{2\Delta m_{21}^2} \cos^2 \theta \right)^2}{\cos^4 \theta (1 + \sin^2 \theta)} \right] \Big|_{x=x_R},
\end{aligned} \tag{74}$$

where we have used various relations in Table II. Hence, given  $\theta$  and  $\phi$ 's minute effects on the adiabatic edge and thus the fitted  $\Delta m_{21}^2$ , if  $\sin^2 2\varphi$  fits the data for the case where  $\theta = \phi$ , the case  $\nu_{1-} \leftrightarrow \nu_{2+}$  with  $\phi = 0$  will be well described by the mixing parameter  $\sin^2 2\theta$ , which is approximately related to  $\sin^2 2\varphi$ , assuming small intergenerational mixing, in the following manner:

$$\begin{aligned}
\sin^2 2\theta &\cong \left( \frac{1}{1 - \frac{|A_{NC}|}{2\Delta m_{21}^2}} \right)^2 \sin^2 2\varphi \cong \left( \frac{1}{1 - \frac{N_n(x_R)}{2N_e(x_R)}} \right)^2 \sin^2 2\varphi \\
&\cong (1.2 \rightarrow 1.8) \sin^2 2\varphi.
\end{aligned} \tag{75}$$

The same analysis applies to the case of  $\nu_{1+} \leftrightarrow \nu_{2-}$ .

## B. Case B2

Case B2 corresponds to

$$\Delta m_{2+2-}^2 \gg \Delta m_{21}^2 \gg \Delta m_{1+1-}^2 \gtrsim 10^{-10} \text{eV}^2. \quad (76)$$

The squared masses of the instantaneous mass eigenstates for the relevant solar densities are shown in Fig. 3. As in Case B1, the evolution of  $\nu_{2h}^m$  is virtually density-independent and thus adiabatic due to a large  $\Delta m_{2+2-}^2$ . To a very good approximation,

$$\nu_{2h}^m = \nu_{2h}, \quad (77)$$

and

$$U_{e2h}^m = U_{e2h}. \quad (78)$$

The decoupling of  $\nu_{2h}$  renders the  $\nu_e$  survival probability into the form:

$$\begin{aligned} P_{ee}^\oplus(E) &= |U_{e2h}|^4 + \left| \sum_{i,j=1\ell,1h,2\ell} U_{ei}^m(x_i) \exp \left[ -i \int_{x_i}^{x_f} \mathcal{H}_{ij}^m dx \right] U_{ej} \right|^2 \\ &= |U_{e2h}|^4 + (1 - |U_{e2h}|^2)^2 P_{3\nu MSW}, \end{aligned} \quad (79)$$

where

$$P_{3\nu MSW} = \left| \sum_{i,j=1\ell,1h,2\ell} \frac{U_{ei}^m}{\sqrt{U_{e1\ell}^{m2} + U_{e1h}^{m2} + U_{e2\ell}^{m2}}} \exp \left[ -i \int_{x_i}^{x_f} \mathcal{H}_{ij}^m dx \right] \frac{U_{ej}}{\sqrt{U_{e1\ell}^2 + U_{e1h}^2 + U_{e2\ell}^2}} \right|^2, \quad (80)$$

and  $U_{e1\ell}^{m2} + U_{e1h}^{m2} + U_{e2\ell}^{m2} = U_{e1\ell}^2 + U_{e1h}^2 + U_{e2\ell}^2$  by unitarity. If we regard the decoupled  $\nu_{2h}^m$  ( $\sim \nu_{2h}$ ) state as containing a fraction  $|U_{e2h}^m|^2$  ( $\sim |U_{e2h}|^2 \sim 0$ ) of the original  $\nu_e$  population, the other  $(1 - |U_{e2h}|^2 \sim 1)$  is thus distributed in the remaining three states. The splittings between these states lie, by assumption, within the MSW range given in Eq.(29), forming a  $3\nu$  subsystem which undergoes, technically, two resonances  $R_H$  and  $R_L$ . In this manner,  $P_{3\nu MSW}$  is equivalent to the  $\nu_e$  survival probability for a standard  $\nu_e \leftrightarrow \nu_\mu \leftrightarrow \nu_\tau$  system with  $m_\tau^2 \gg m_\mu^2 \simeq m_e^2$  [25,28,31,32] (plus some non-standard features due to the presence of sterile neutrinos). Contrary to the standard  $3\nu$  system where the spotlight is on  $R_L$ , and  $R_H$  occurs at too high a density to be relevant, our focus is on  $R_H$ . (We do not consider  $R_L$  because the close encounter of the mass eigenvalues of  $\nu_{1\ell}^m$  and  $\nu_{1h}^m$  in Fig. 3 represents maximal conversion of  $\nu_e$  into  $\nu'_e$ . This happens in vacuum, necessarily adiabatically.)

Standard  $3\nu$  systems have been studied extensively [25,28,31,32]. Following from these analyses, we parameterise the following mixing angles:

$$\begin{aligned} \cos \psi_m &= \frac{U_{e1\ell}^m}{\sqrt{U_{e1\ell}^{m2} + U_{e1h}^{m2}}}, \quad \sin \psi_m = \frac{U_{e1h}^m}{\sqrt{U_{e1\ell}^{m2} + U_{e1h}^{m2}}}, \\ \cos \eta_m &= \sqrt{\frac{U_{e1\ell}^{m2} + U_{e1h}^{m2}}{U_{e1\ell}^{m2} + U_{e1h}^{m2} + U_{e2\ell}^{m2}}}, \quad \sin \eta_m = \frac{U_{e2\ell}^m}{\sqrt{U_{e1\ell}^{m2} + U_{e1h}^{m2} + U_{e2\ell}^{m2}}}, \end{aligned} \quad (81)$$

where the subscripts and superscripts  $m$  denote their density-dependent counterparts. The angle  $\psi_m$  describes (approximately) the mixing of  $\nu_e$  and  $\nu'_e$ , and takes on a value of  $\psi_m = \psi \cong \frac{\pi}{4}$  in vacuum. This mixing mode is strongly suppressed at high densities because of the small vacuum splitting between  $\nu_{1\ell}$  and  $\nu_{1h}$  (so that  $\psi_m \rightarrow \frac{\pi}{2}$  as  $\rho \rightarrow \infty$ ). Consequently, the  $\nu_1$  state that takes part in the intergenerational MSW resonance  $R_H$  at density  $\rho \sim \Delta m_{21}^2$  resembles neither  $\nu_{1\ell}$  nor  $\nu_{1h}$  but is, asymptotically, some approximately maximal linear combinations of the two states, which we denote as  $\nu_{1x}$ . Its orthogonal state,  $\nu_{1y}$ , is thus the asymptotic form of  $\nu_{1\ell}^m$  for the relevant solar densities, that is,

$$\begin{pmatrix} \nu_{1x} \\ \nu_{1y} \\ \nu_{2\ell} \\ \nu_{2h} \end{pmatrix} = \mathcal{O}(\psi) \begin{pmatrix} \nu_{1\ell} \\ \nu_{1h} \\ \nu_{2\ell} \\ \nu_{2h} \end{pmatrix} = \begin{pmatrix} \cos \psi & \sin \psi & 0 & 0 \\ -\sin \psi & \cos \psi & 0 & 0 \\ 0 & 0 & 1 & 0 \\ 0 & 0 & 0 & 1 \end{pmatrix} \begin{pmatrix} \nu_{1\ell} \\ \nu_{1h} \\ \nu_{2\ell} \\ \nu_{2h} \end{pmatrix}. \quad (82)$$

Note that for small intergenerational mixing,  $\nu_{1x} \simeq \nu_e$  and  $\nu_{1y} \simeq \nu'_e$  by Eqs. (81) and (82). At density  $0 \ll \rho \ll \rho_{R_H}$ , we may treat the  $4\nu$  system as consisting of two parity eigenstates  $\nu_{2\ell}$  and  $\nu_{2h}$ , and two pseudo-mass eigenstates  $\nu_{1x}$  and  $\nu_{1y}$  of indefinite parity.

The angle  $\eta$  describes the *apparent* mixing of  $\nu_{1x}$  and  $\nu_{2\ell}$  in vacuum, which is minimal as inferred from Eqs.(32) and (81) assuming small intergenerational mixing. However, in the proximity of  $R_H$  (at  $\rho \sim \Delta m_{21}^2$ ), while  $\nu_{1y}$  and  $\nu_{2h}$  propagate virtually density-independently, matter effects rotate  $\eta_m$  from its vacuum value  $\eta$  through  $\frac{\pi}{4}$  to  $\frac{\pi}{2}$ , and thereby modify the evolution of  $\nu_{1x}$  and  $\nu_{2\ell}$  dramatically. If we regard  $\nu_{1x}$  and  $\nu_{2\ell}$  as forming two orthogonal pseudo-weak eigenstates  $\nu_a$  and  $\nu_b$  that convert resonantly into each other at  $R_H$ , i.e.,

$$\begin{aligned} \begin{pmatrix} \nu_a \\ \nu_{1y} \\ \nu_b \\ \nu_{2h} \end{pmatrix} &= \mathcal{S}(\eta) \begin{pmatrix} \nu_{1x} \\ \nu_{1y} \\ \nu_{2\ell} \\ \nu_{2h} \end{pmatrix} = \begin{pmatrix} \cos \eta & 0 & \sin \eta & 0 \\ 0 & 1 & 0 & 0 \\ -\sin \eta & 0 & \cos \eta & 0 \\ 0 & 0 & 0 & 1 \end{pmatrix} \begin{pmatrix} \nu_{1x} \\ \nu_{1y} \\ \nu_{2\ell} \\ \nu_{2h} \end{pmatrix} \\ &= \mathcal{S}(\eta) \mathcal{O}(\psi) \begin{pmatrix} \nu_{1\ell} \\ \nu_{1h} \\ \nu_{2\ell} \\ \nu_{2h} \end{pmatrix} = \begin{pmatrix} \cos \eta \cos \psi & \cos \eta \sin \psi & \sin \eta & 0 \\ -\sin \psi & \cos \psi & 0 & 0 \\ -\sin \eta \cos \psi & -\sin \eta \sin \psi & \cos \eta & 0 \\ 0 & 0 & 0 & 1 \end{pmatrix} \begin{pmatrix} \nu_{1\ell} \\ \nu_{1h} \\ \nu_{2\ell} \\ \nu_{2h} \end{pmatrix}, \end{aligned} \quad (83)$$

we may follow a similar procedure to Eqs.(52) and (53) and approximate  $U^m$  as

$$U^m = U \mathcal{O}^{-1}(\psi) \mathcal{S}^{-1}(\eta) \mathcal{S}(\eta_m) \mathcal{O}(\psi_m), \quad (84)$$

such that the effective Hamiltonian that governs the evolution of  $\nu_a$  and  $\nu_b$  in the vicinity of  $R_H$  is given by the  $1 - 3$  sector of

$$\begin{aligned} \mathcal{H}_{eff} &= \frac{1}{2E} [\mathcal{S}(\eta) \mathcal{O}(\psi) \mathcal{M} \mathcal{O}^{-1}(\psi) \mathcal{S}^{-1}(\eta) + \mathcal{S}(\eta) \mathcal{O}(\psi) U^{-1} \mathcal{H}_{int} U \mathcal{O}^{-1}(\psi) \mathcal{S}^{-1}(\eta)] \\ &\xrightarrow{1-3sector} \frac{1}{4} \begin{pmatrix} -\Delta m_{eff}^2 \cos 2\eta + A_{eff} & \Delta m_{eff}^2 \sin 2\eta + A_{ind} \\ \Delta m_{eff}^2 \sin 2\eta + A_{ind} & \Delta m_{eff}^2 \cos 2\eta - A_{eff} \end{pmatrix} + \text{constant}, \end{aligned} \quad (85)$$

where

$$\Delta m_{eff}^2 \equiv m_{2\ell}^2 - \frac{1}{2}(m_{1\ell}^2 + m_{1h}^2 - \Delta m_{1+1-}^2 \cos 2\psi) \cong m_{2\ell}^2 - \bar{m}_1^2. \quad (86)$$

The term  $\Delta m_{eff}^2$  represents the effective vacuum squared mass difference responsible for the resonance, and  $\bar{m}_1^2$  is the averaged squared mass of the  $\nu_1$  states,  $\bar{m}_1^2 = \frac{1}{2}(m_{1\ell}^2 + m_{1h}^2)$ . The magnitudes of  $\Delta m_{eff}^2$  and  $\Delta m_{21}^2$ , where  $\Delta m_{21}^2 = m_{2\ell}^2 - m_{1h}^2$ , are virtually identical. Henceforth, we shall replace  $\Delta m_{eff}^2$  with  $\Delta m_{21}^2$  whenever the former is encountered for convenience. The quantities  $A_{eff}$  and  $A_{ind}$  are given by

$$\begin{aligned} A_{eff} = & A_{CC}(U_{e1\ell}^2 + U_{e1h}^2 + U_{e2\ell}^2) \\ & + A_{NC}\{\cos 2\eta[(\cos \psi U_{e1\ell} + \sin \psi U_{e1h})^2 - U_{e2\ell}^2 + (\cos \psi U_{\mu 1\ell} + \sin \psi U_{\mu 1h})^2 - U_{\mu 2\ell}^2] \\ & + 2\sin 2\eta[U_{e2\ell}(\cos \psi U_{e1\ell} + \sin \psi U_{e1h}) + U_{\mu 2\ell}(\cos \psi U_{\mu 1\ell} + \sin \psi U_{\mu 1h})]\}, \end{aligned} \quad (87)$$

and

$$\begin{aligned} A_{ind} = & A_{NC}\{2\cos 2\eta[U_{e2\ell}(\cos \psi U_{e1\ell} + \sin \psi U_{e1h}) + U_{\mu 2\ell}(\cos \psi U_{\mu 1\ell} + \sin \psi U_{\mu 1h})] \\ & - \sin 2\eta[(\cos \psi U_{e1\ell} + \sin \psi U_{e1h})^2 - U_{e2\ell}^2 + (\cos \psi U_{\mu 1\ell} + \sin \psi U_{\mu 1h})^2 - U_{\mu 2\ell}^2]\}, \end{aligned} \quad (88)$$

respectively. Table III shows  $A_{eff}$  and  $A_{ind}$  evaluated for various combinations of  $\nu_{1\ell}$ ,  $\nu_{1h}$  and  $\nu_{2\ell}$ .

Taking the well-established  $3\nu$  survival probability from Ref. [25] and setting the level-crossing probability at  $R_L$  to zero, we may immediately write down  $P_{3\nu MSW}$  as

$$\begin{aligned} P_{3\nu MSW} = & \sin^2 \eta_m(x_i) \sin^2 \eta + \cos^2 \eta_m(x_i) \cos^2 \eta [\sin^2 \psi_m(x_i) \sin^2 \psi + \cos^2 \psi_m(x_i) \cos^2 \psi] \\ & - P_{R_H} [\sin^2 \eta_m(x_i) - \cos^2 \eta_m(x_i) \sin^2 \psi_m(x_i)] (\sin^2 \eta - \cos^2 \eta \sin^2 \psi), \end{aligned} \quad (89)$$

where  $P_{R_H}$  is the level-crossing probability at resonance  $R_H$  calculated from  $\mathcal{H}_{eff}$  in Eq.(85). Furthermore, because of the strong suppression of  $\nu_e \leftrightarrow \nu'_e$  oscillations in most parts of the sun, the corresponding matter mixing angle  $\psi_m$  is close to  $\frac{\pi}{2}$ , thereby reducing Eq.(89) to

$$\begin{aligned} P_{3\nu MSW} = & \sin^2 \eta_m(x_i) \sin^2 \eta + \cos^2 \eta_m(x_i) \cos^2 \eta \sin^2 \psi \\ & - P_{R_H} [\sin^2 \eta_m(x_i) - \cos^2 \eta_m(x_i)] (\sin^2 \eta - \cos^2 \eta \sin^2 \psi). \end{aligned} \quad (90)$$

Equation (90) does not present itself in the most illuminating for the purpose of comparison. In the first instance, it does not, superficially, resemble the familiar expression for the standard  $2\nu$  MSW transition probability  $P_{2\nu MSW}$  in Eq.(41). However, putting it into context, the overall  $\nu_e$  survival probability  $P_{ee}^\oplus(E)$  for Case B2 in Eq.(79) can be recast into

$$P_{ee}^\oplus(E) = |U_{e2h}|^4 + (1 - |U_{e2h}|^2)(1 - |U_{e1\ell}|^2 - |U_{e2\ell}|^2)\tilde{P}_{2\nu MSW}, \quad (91)$$

where

$$\tilde{P}_{2\nu MSW} = \frac{1}{2} + \left(\frac{1}{2} - P_{R_H}\right) \cos 2\eta_m(x_i) \cos 2\omega, \quad (92)$$

and

$$\cos \omega = \frac{U_{e1h}}{\sqrt{U_{e1h}^2 + U_{e2\ell}^2}}, \quad \sin \omega = \frac{U_{e2\ell}}{\sqrt{U_{e1h}^2 + U_{e2\ell}^2}}. \quad (93)$$

In the limit of small intergenerational mixing,  $\tilde{P}_{2\nu MSW} \rightarrow P_{2\nu MSW}$  in such a way that Eq.(91) is well approximated by

$$P_{ee}^\oplus(E) \approx \frac{1}{2} P_{2\nu MSW}, \quad (94)$$

where  $P_{2\nu MSW}$  is evaluated for  $\Delta m_{21}^2$  and  $\eta$  in a medium of effective density

$$A_{eff} \approx A_{CC} + \frac{1}{2} A_{NC}, \quad (95)$$

as inferred from Table III, with a level-crossing probability  $P_{RH}$  governed by  $\mathcal{H}_{eff}$  in Eq.(85). Given the respective standard  $\nu_e \leftrightarrow \nu_{\mu,\tau}$  and  $\nu_e \leftrightarrow \nu_s$  effective densities:

$$\begin{aligned} A_{eff}(\nu_e \leftrightarrow \nu_{\mu,\tau}) &= A_{CC}, \\ A_{eff}(\nu_e \leftrightarrow \nu_s) &= A_{CC} + A_{NC}, \end{aligned} \quad (96)$$

Eq.(95) immediately puts the adiabatic edge of the MSW transition between that of the two standard cases for the same oscillation parameters as shown in Fig. 4.

On the non-adiabatic aspect of  $P_{2\nu MSW}$ , we learn from Table III that the mixing angle  $\eta$  and the off-diagonal term  $A_{ind}$  (both of which appear in the level-crossing probability) do not distinguish between the exact identities of  $\nu_{1\ell}$  and  $\nu_{1h}$ , or equivalently, the sign of  $\Delta m_{1+1-}^2$ . (They do, however, depend on the identity of  $\nu_{2\ell}$  — a matter of interchanging  $\theta$  and  $\phi$ .) This is because the enhanced *apparent* mixing mode at  $R_H$  is that of  $\nu_{1x} \leftrightarrow \nu_{2\ell}$ . The state  $\nu_{1x}$ , in turn, is a fixed,  $\Delta m_{1+1-}^2$  independent admixture of  $\nu_{1+}$  and  $\nu_{1-}$ , such that  $\Delta m_{1+1-}^2$  does not enter the scene so long as Eq.(76) is satisfied. The matter-induced mixing term  $A_{ind}$  varies with  $\theta$  and  $\phi$ . Taking the case of  $\nu_{1x} \leftrightarrow \nu_{2-}$ , we observe that  $A_{ind}$  vanishes exactly when  $\theta = 0$ . For  $\theta = \phi$ , we have  $A_{ind} = -\frac{|A_{NC}|}{2} \sin 2\eta = \frac{|A_{NC}|}{2} \sin 2\eta$  so that the ratio of matter-induced to vacuum mixing evaluated at resonance is given by

$$\Lambda = \frac{|A_{NC}|}{2\Delta m_{21}^2} = \frac{\cos 2\eta}{4 \left( \frac{N_e(x_R)}{N_n(x_R)} \right) - 1} \approx 0.04 \rightarrow 0.14. \quad (97)$$

The contribution of matter-induced mixing (which is additive here by definition) is therefore relatively small. Given an effective density in Eq.(95) that is almost independent of  $\theta$  and  $\phi$  (provided they are small), approximately the same  $\Delta m_{21}^2$  will provide a fit to the experimental data for any combination of  $\theta$  and  $\phi$ . It then follows from Eq.(97) that for the  $\theta = \phi$  case,  $\sin^2 2\eta$  lies in the range

$$\sin^2 2\eta \approx (0.8 \rightarrow 0.9) \sin^2 2\varphi, \quad (98)$$

where  $\sin^2 2\varphi$  is the fitted mixing parameter for the case where no matter-induced mixing is present (i.e., when  $\theta = 0$ ). At the other extreme, Table III shows that for  $\nu_{1x} \leftrightarrow \nu_{2-}$ , matter-induced mixing takes full control if  $\phi = 0$ . This mixing, however, is negligible. Following from Eqs.(64) to (66), the quantity  $\kappa^2(x)$  that appears in the level-crossing probability is now proportional to  $A_{ind}^2$ , i.e.,

$$\begin{aligned}
(|A_{NC}| \cos 2\eta \cos \alpha \sin \theta)^2 &= (\Delta m_{21}^2)^2 \sin^2 2\theta \left( \frac{|A_{NC}|}{2\Delta m_{21}^2} \right)^2 \frac{1}{\cos^2 \theta + 1} \\
&\approx (8 \times 10^{-4} \rightarrow 10^{-2}) (\Delta m_{21}^2)^2 \sin^2 2\theta.
\end{aligned} \tag{99}$$

Thus, given that  $\sin^2 2\theta$  is sufficiently small, the level-crossing probability for  $\phi = 0$  is almost one. [If the resonance is sufficiently close to the centre of the sun where  $\frac{N_e}{N_n} \sim 2$ , matter-induced mixing may show itself by contributing to the level-crossing probability an equivalent of  $\sin^2 2\theta \times 10^{-2}$  by Eq.(99).]

We may carry out the same analysis for  $\nu_{1x} \leftrightarrow \nu_{2+}$ , which involves little more than interchanging  $\theta$  and  $\phi$ .

### C. Case C

Case C comprises the following parameters:

$$\Delta m_{2+2-}^2 \gg \Delta m_{21}^2 \gg \Delta m_{1+1-}^2, \Delta m_{1+1-}^2 \lesssim 10^{-11} eV^2. \tag{100}$$

The mathematics that describes the resonant conversion of  $\nu_e$  in the interior of the sun for this case is identical to that for Case B2 where the resonance  $R_H$  is one of enhanced  $\nu_{1x} \leftrightarrow \nu_{2\ell}$  mixing. Indeed, the two systems are physically identical. However, the suppression of  $\nu_e \leftrightarrow \nu'_e$  oscillations is no longer solely a matter effect but is extended to the vacuum, leading to a vastly different phenomenology. Vacuum  $\nu_e \leftrightarrow \nu'_e$  oscillations do not happen because of the extremely small  $\Delta m_{1+1-}^2$  which in turn corresponds to an oscillation length much longer than an astronomical unit. We may therefore treat the problem as though the lower resonance  $R_L$  (responsible for  $\nu_e \leftrightarrow \nu'_e$ ) in Fig. 3 is completely absent. The  $\nu_e$  survival probability is then given by Eq.(79) with  $P_{3\nu MSW}$  replaced with  $P_{2\nu MSW}$ , i.e.,

$$P_{ee}^\oplus(E) = |U_{e2h}|^4 + (1 - |U_{e2h}|^2)^2 P_{2\nu MSW}. \tag{101}$$

The MSW transition probability  $P_{2\nu MSW}$  is that in Eq.(41) evaluated for the effective Hamiltonian of Case B2 in Eq.(85) with a squared mass difference  $\Delta m_{eff}^2 \cong \Delta m_{21}^2$  and mixing angle  $\eta$  defined in Eqs.(86) and (81) respectively. Assuming small intergenerational mixing, Eq.(101) reduces to

$$P_{ee}^\oplus(E) \approx P_{2\nu MSW}, \tag{102}$$

where  $P_{2\nu MSW}$  contains non-standard features as described earlier for Case B2. Equation (102) is represented graphically in Fig. 5.

## IV. SOLUTIONS TO THE SOLAR NEUTRINO PROBLEM

In this section, we locate the regions of parameter space that will give rise to the observed solar neutrino depletion for Cases B1, B2 and C in an approximate way. Currently available experimental data suggest a significant depletion of the mid-energy neutrinos, hinting at a pre-defined shape for the  $\nu_e$  survival probability. By going to regions of parameter space in

which matter-induced mixing is small, the approximate  $\nu_e$  survival probabilities in Eqs.(63), (94) and (102) for Cases B1, B2 and C respectively are very simply related to the standard two-flavour  $P_{2\nu MSW}$ . Thus, by comparison with the standard solutions, we may gain a rough feeling for the necessary oscillations parameters for each case without performing an *ab initio* fit to the experimental data.

Flux-independent data from Kamiokande and SuperKamiokande such as spectral distortion and day-night asymmetry provide yet another means to identify the allowed oscillation parameters [33–35]. Although the day-night effect is beyond the scope of this paper, we will be able to comment on the expected spectral distortion in Cases B1, B2 and C.

### A. Case B1

Let us reiterate that the oscillation parameters for Case B1 are constrained by Eqs.(43) and (44). For comparison, it is useful to define the ratio of the event rate with oscillations to that with no oscillations as

$$\Omega = \frac{\int_{E_0}^{\infty} \overline{P}_{ee}^{\oplus}(E) \phi_0^{\oplus}(e, E) \sigma(E) dE}{\int_{E_0}^{\infty} \phi_0^{\oplus}(e, E) \sigma(E) dE}, \quad (103)$$

where  $\phi_0^{\oplus}(e, E)$  is the no-oscillation  $\nu_e$  flux,  $\sigma(E)$  is the detection cross-section,  $E_0$  is the experimental energy threshold, and  $\overline{P}_{ee}^{\oplus}(E)$  is the  $\nu_e$  survival probability averaged over production positions. By Eq.(63), the energy-dependence of the  $\nu_e$  survival probability for this case is contained entirely in the term  $P_{2\nu MSW}$ . In the small intergenerational mixing limit, we further approximate the adiabatic edge of  $P_{2\nu MSW}$  as a step function  $\theta(E_A^{4\nu} - E)$ , where  $E_A^{4\nu}$  is  $E_A$  defined in Eq.(62), such that

$$P_{2\nu MSW}|_{4\nu} \cong \theta(E_A^{4\nu} - E) + P_R^{4\nu}. \quad (104)$$

For comparison purposes, we also write down an analogous expression for a  $2\nu$  system:

$$P_{2\nu MSW}|_{2\nu} \cong \theta(E_A^{2\nu} - E) + P_R^{2\nu}, \quad (105)$$

where

$$E_A^{2\nu} = \frac{\Delta m_{21}^2 \cos 2\eta}{2\sqrt{2}G_F N_e(x_i)}. \quad (106)$$

Equation (106) comes from the resonance condition,  $A_{eff} = A_{CC} = \Delta m_{21}^2 \cos 2\eta$ , for a standard  $\nu_e \leftrightarrow \nu_{\mu, \tau}$  system, and a comparison with Eq.(62) immediately leads us to

$$2E_A^{2\nu} \cong E_A^{4\nu}. \quad (107)$$

The scale heights  $\left| \frac{1}{A_{eff}} \frac{dA_{eff}}{dt} \right|$  that appear in the level-crossing probabilities  $P_R^{4\nu}$  and  $P_R^{2\nu}$  do not differ much due to the almost exponential solar density profile [21]. Thus, if we ignore matter-induced mixing by setting  $\theta = \phi$  according to Table II, we may make the approximation:

$$P_R^{4\nu} \cong P_R^{2\nu}, \quad (108)$$

such that, by Eqs.(63), (103 – 105) and (107),

$$\Omega_{4\nu}(\Delta m^2, \sin^2 2\eta) \simeq \frac{1}{4} + \frac{1}{4}\Omega_{2\nu}(2\Delta m^2, \frac{1}{2}\sin^2 2\eta). \quad (109)$$

Here,  $\Omega_{4\nu}(\Delta m^2, \sin^2 2\eta)$  denotes the value of  $\Omega$  in our  $4\nu$  scheme evaluated for  $\Delta m^2$  and  $\sin^2 2\eta$ , and  $\Omega_{2\nu}(2\Delta m^2, \frac{1}{2}\sin^2 2\eta)$  is the ratio  $\Omega$  in the standard  $\nu_e \leftrightarrow \nu_{\mu, \tau}$  scheme evaluated at twice the squared mass difference and half the mixing. The rescaling of  $\Delta m^2$  and  $\sin^2 2\eta$  in the latter is dictated by Eq.(108), such that the parameter  $\Delta m^2 \sin^2 2\eta$  that is fed into  $P_R^{4\nu}$  and  $P_R^{2\nu}$  respectively agree. Thus, in the extreme case of  $\Delta m_{1+1-}^2 \sim 10^{-3} eV^2$ , a minimum of  $\frac{1}{4}$  of the original neutrino flux must be detected, while the maximum detectable flux is  $\frac{1}{2}$  as a direct consequence of maximal vacuum  $\nu_e \leftrightarrow \nu'_e$  oscillations. The latter corresponds to the absence of MSW transitions, or equivalently, to  $\Delta m_{21}^2$  and  $\eta$  residing in regions of parameter space outside of that quoted in Eqs.(29) and (30) respectively.

Equation (109) allows us to virtually fit the experimental data by the use of existing theoretical  $\nu_e \leftrightarrow \nu_{\mu, \tau}$  predictions for the various experiments in which smearing over production point and other energy dependence are already accounted for. Given a set of standard  $2\nu$  MSW contours, we can pick out the necessary oscillation parameters for this case graphically by identifying each  $\Omega_{2\nu}$  contour with a  $\Omega_{4\nu}$  by Eq.(109), and adjusting the  $\Delta m^2$  and  $\sin^2 2\eta$  scales accordingly. The area enclosed by the dot-dash line in Fig. 6 represents the region of parameter space in which the  $2\sigma$  bands (including both experimental and theoretical errors) of all five experiments overlap [36]. Numerically, this region is defined by

$$2 \times 10^{-6} \lesssim \Delta m_{21}^2 / eV^2 \lesssim 5 \times 10^{-5}, \quad (110)$$

and

$$8 \times 10^{-4} \lesssim \sin^2 2\eta \lesssim 0.1. \quad (111)$$

[Beyond  $\sin^2 2\eta \sim 0.1$ , Eqs.(63) and (109) become invalid as intergenerational vacuum oscillations increase in amplitude.] Note that our fitting procedure is approximate, but should nevertheless yield a solid indication of the  $2\sigma$  allowed parameter space. We also find that the  $1\sigma$  bands do not overlap in this case, suggesting that the solution is not acceptable at below 68% C. L.. Figure 7 shows the  $\nu_e$  survival probability for several representative sets of oscillation parameters within the allowed region for Case B1.

A qualitative discussion of this virtual fit follows. Firstly, from Eq. (16), to Table I, large uncertainties in the Boron flux means that Kamiokande and SuperKamiokande's  $2\sigma$  bands necessarily span the entire region of MSW parameter space for this case. Secondly, the central values of the GALLEX and SAGE results are somewhat higher than the maximum detectable ratio of  $\frac{1}{2}$  as predicted by the EPM. Hence, the lower bound on  $\Delta m_{21}^2$  is set by the Gallium experiments, corresponding to the maximum amount of low- and mid-energy neutrinos that can be killed resonantly within limits.

The central value of the Homestake result is  $\sim \frac{1}{4}$  relative to SSM prediction, while at plus  $2\sigma$ , the ratio of measured to no-oscillation event rates does not quite reach the maximum of  $\frac{1}{2}$ . Thus, the upper bound on the squared mass difference  $\Delta m_{21}^2$  and the lower bound on

$\Delta m_{21}^2 \sin^2 2\eta$  are determined by Homestake, representing the possible suppression patterns that the Boron spectrum may receive.

Note that we have arrived at these assuming  $\theta = \phi$ . A rough indication of the necessary regions of parameter space for cases of unequal  $\theta$  and  $\phi$  can be obtained based on the analyses in Sec. III. In short, unequal  $\theta$  and  $\phi$  will give more breadth to the allowed region.

## B. Case B2

In Case B2, the parameters are constrained by Eq.(76). The  $\nu_e$  survival probability for this case in Eq.(91) consists of negligible constant terms due to averaged vacuum oscillations. This is a direct consequence of the strong suppression of  $\nu_e \leftrightarrow \nu'_e$  oscillations in matter such that almost all of the original  $\nu_e$ 's produced at  $\rho \gg \rho_R$  will pass through a resonance. In this case,  $P_{ee}^\oplus(E)$  plunges down to as low as  $\sim 0$  immediately to the high-energy end of the adiabatic edge according to Eq.(94) and Fig. 4. The correspondingly deeper pit in  $P_{2\nu MSW}$  implies that the adiabatic edge needs to occur at an even higher energy in order to maximise the number of low- and mid-energy neutrinos to be detected. This is attainable by choosing an even higher squared mass difference.

The naturally smaller-than-standard effective density in Eq.(95) places the adiabatic edge of Case B2 at a somewhat higher energy. The exact location of the edge relative to a standard edge, however, cannot be simply quantified since  $N_e(x)$  and  $N_n(x)$  do not exactly track each other in the sun. However, expressing  $A_{eff}$  of Eq.(95) in terms of  $A_{CC}$  for the relevant solar densities,

$$A_{eff} \approx \left(\frac{7}{8} \rightarrow \frac{23}{24}\right) A_{CC}, \quad (112)$$

the shift of the adiabatic edge relative to the standard location is negligible. On the non-adiabatic side, if we neglect matter-induced mixing (by setting  $\theta = 0$  for  $\nu_{1x} \leftrightarrow \nu_{2-}$ , or  $\phi = 0$  for  $\nu_{1x} \leftrightarrow \nu_{2+}$ ),  $P_R^{4\nu}$  evaluated for this case will be approximately the same as  $P_R^{2\nu}$  for a standard  $2\nu$  system with the same  $\Delta m^2$  and  $\eta$ . Hence,  $P_{2\nu MSW}|_{4\nu} \approx P_{2\nu MSW}|_{2\nu}$  and

$$\Omega_{4\nu}(\Delta m^2, \sin^2 2\eta) \approx \frac{1}{2} \Omega_{2\nu}(\Delta m^2, \sin^2 2\eta), \quad (113)$$

by Eqs.(94) and (103), and the symbols carry the same definitions as before. Thus, utilising established  $2\nu$  MSW transition probability contours, we obtain the allowed oscillation parameters for Case B2 by Eq.(113) in a region defined by

$$10^{-5} \lesssim \Delta m_{21}^2 / eV^2 \lesssim 10^{-4}, \quad (114)$$

and

$$10^{-4} \lesssim \sin^2 2\eta \lesssim 4 \times 10^{-3}, \quad (115)$$

including both experimental and theoretical errors at  $2\sigma$  as shown in Fig. 6. This is a considerably smaller region than that for Case B1. In particular, the Kamiokande and SuperKamiokande results now place an upper bound on the allowed  $\sin^2 2\eta$  such that we do not wipe out too many Boron neutrinos by the MSW mechanism in the non-adiabatic branch. The  $\nu_e$  survival probability for this case for several representative sets of oscillation parameters within the allowed region is shown in Fig. 8.

### C. Case C

Case C is described by the parameters given in Eq.(100). In view of Fig. 5, the similarity between the energy-dependences of this case and of the standard  $2\nu$  (both  $\nu_e \leftrightarrow \nu_{\mu,\tau}$  and  $\nu_e \leftrightarrow \nu_s$ ) scenarios shows that due to the absence of vacuum  $\nu_e \leftrightarrow \nu'_e$  oscillations, the necessary oscillation parameters for Case C will lie in between those of the two standard cases (see Table IV). The solution at 95% C. L. is shown in Fig. 6.

## V. PROSPECTS FOR FUTURE EXPERIMENTS

We now briefly discuss the implications of the various solutions on experimental observables. In particular, we shall look at the Boron energy spectrum observed by the high-energy scattering experiments, the Beryllium line that will be detected by BOREXINO, and the charged to neutral current event rates to be measured by SNO.

### A. Boron spectral distortion

Qualitatively, the underlying maximal  $\nu_e \leftrightarrow \nu'_e$  vacuum oscillations in Cases B1 and B2 will lead to recoil electron energy spectra for SuperKamiokande and SNO respectively that are almost flat with respect to SSM predictions. This can be seen by comparing the various survival probabilities in Figs. 7 and 8. For Case B1 (Fig. 7), the energy-independent  $\frac{1}{4}$  that provides a lower limit to the flux depletion considerably softens the energy-dependence of the non-adiabatic branch of the  $\nu_e$  survival probability. For Case B2 (Fig. 8), the slope of the non-adiabatic branch is scaled down by a factor of two, relative to the standard MSW solutions, because of Eq.(94). For Case A, complete energy-dependence means that spectral distortion is absent as in the no-oscillation case. Precise predictions for the amount of deformation in energy-dependent cases relative to standard expectations cannot be obtained without performing an *ab initio* numerical fit, because of the vastly different oscillation parameters involved. However, it may be said for certain that the spectral distortions in Cases B1 and B2 are significantly weaker than those predicted by all other minimal  $\nu_e \leftrightarrow \nu_{\mu,\tau}$  and/or  $\nu_e \leftrightarrow \nu_s$  schemes currently in the market [38], and are somewhat stronger than the standard large mixing angle (LMA) scheme.

Based on  $\frac{\Delta T}{T}$ , the deviation of the averaged measured electron kinetic energy from its standard value, SuperKamiokande's flux-independent data to date do not distinguish between the standard  $2\nu$  small mixing angle, the large mixing angle and the no-oscillation solutions within  $1\sigma$  [35]. From Figs. 7 and 8, we expect the quantities  $\frac{\Delta T}{T}$  resulting from Cases B1 and B2 respectively to take on some intermediate values, compared with the standard SMA and LMA solutions. In this respect, Cases B1 and B2 are consistent with spectral data to date. Case A is also acceptable. (A small reduction in the allowed regions for Cases B1 and B2 displayed in Fig. 6 may result from a rigorous consideration of existing spectral distortion data. If this were to occur, its cause would be the encroachment of the adiabatic edge above the energy threshold for SuperKamiokande, which is presently  $\sim 6.5$  MeV. An inspection of Figs. 7 and 8, however, reveals that the adiabatic edges occur at less than 6.5 MeV in our admittedly approximate fits.)

Observational effects associated with Case C are similar to those studied in Ref. [7]. This case will give a recoil electron energy spectrum that is similar to that predicted by the standard  $2\nu$  cases. Currently available flux-dependent and flux-independent data do not distinguish between this case and the standard  $\nu_e \leftrightarrow \nu_{\mu,\tau}$  and  $\nu_e \leftrightarrow \nu_s$  SMA scenarios. However, the SMA solution is preferred by SuperKamiokande over the LMA solution based on spectral data analyses [35]. To this end, Case C looks promising.

## B. The Beryllium line

With the exception of Case C which predicts an energy-dependence that is similar to the standard  $\nu_e \leftrightarrow \nu_{\mu,\tau}$  and  $\nu_e \leftrightarrow \nu_s$  scenarios, maximal vacuum  $\nu_e \leftrightarrow \nu'_e$  oscillations lead to a Beryllium line that must be detected at  $\sim \frac{1}{4}$  to  $\sim \frac{1}{2}$  the no-oscillation rate by BOREXINO. These deductions come from an inspection of Figs. 7 and 8. In particular, if Case B2 is valid, the Beryllium flux will be almost exactly halved, independent of the intergenerational oscillation parameters (provided they lie within the allowed region shown in Fig. 6). In this respect, Cases B1 and B2 are clearly distinguishable from the standard  $2\nu$  SMA schemes. Needless to say, Case A being energy-independent will exactly halve the Beryllium flux.

## C. Charged to neutral current rate

In Sec. II, we obtained a range of the ratio of charged to neutral current event rate at SNO for each of our several cases, based on flux-dependent data from SuperKamiokande alone. Having identified in Secs. III and IV the allowed shapes of the various  $\nu_e$  survival probabilities *which are now constrained by five experiments*, we may narrow these ranges, using expressions developed in Sec. II. We will approximate the energy-averaged  $\nu_e$  survival probability  $\langle P_{ee}^\oplus \rangle$  as the  $P_{ee}^\oplus(E)$  evaluated at an energy of 10MeV for our various cases. The ratios  $r_d$  are shown in Table V.

Considerable overlapping between the ranges for Cases B1, B2 and C means that  $r_d$  is perhaps not the best experimental observable for their disentanglement. However, by measuring  $r_d$  alone, these cases are clearly distinguishable from the standard  $2\nu$  scenarios, both pure active and pure sterile, and from Case A.

## VI. SUMMARY AND CONCLUSIONS

In order to account for the significant depletion of solar neutrinos measured by five experiments to date, we have invoked MSW-enhanced intergenerational mixing in addition to maximal vacuum  $\nu_e \leftrightarrow \nu'_e$  oscillations prescribed by the EPM. Approximate analytical expressions for the  $\nu_e$  survival probabilities as functions of neutrino energy have been obtained for several possible neutrino mass hierarchies assuming small vacuum intergenerational mixing. These expressions were then compared with well-established  $2\nu$  solutions to identify the approximate regions of parameter space that can simultaneously explain the apparent solar and atmospheric neutrino anomalies. (Note that only those parameter space regions which

feature small matter-induced mixing were examined in depth. The approximate allowed regions plotted in Fig. 6 assume this restriction. Some indication of the effect of non-negligible matter-induced mixing is discussed in Sec. III.) The  $\nu_e$  survival probabilities for the Cases A, B1, B2 and C considered herein exhibit considerable differences from each other and from the standard  $\nu_e \leftrightarrow \nu_{\mu, \tau}$  and  $\nu_e \leftrightarrow \nu_s$  small and large mixing cases.

These new, distinguishing features are, in principle, observable by future solar neutrino experiments, and have been briefly discussed. The results are summarised in Table V. By utilising Boron neutrino spectral distortion, the Beryllium neutrino flux and the ratio of charged to neutral current event rates, all the EPM possibilities can be distinguished from the standard  $2\nu$  MSW solutions. The four cases within the EPM also yield different outcomes, except for Cases B1 and B2 which exhibit an overlap for these solar neutrino observables. Fortunately, Cases B1 and B2 can be differentiated through atmospheric neutrino data. The large  $\Delta m_{1+1-}^2$  that defines Case B1 leads to significant  $\nu_e \leftrightarrow \nu'_e$  atmospheric neutrino oscillations. This case is actually already disfavoured by the recent atmospheric neutrino data from SuperKamiokande (see Ref. [39] for detailed discussions). Note that Case C within in the EPM is very similar to the scenario analysed in Ref. [7].

We should also note that the implications of MSW solutions within the EPM for the day-night effect have yet to be examined. In addition, one relevant region of parameter space has not been explored in detail in this paper:  $\Delta m_{1+1-}^2$  values in the approximate range  $10^{-6} \rightarrow 10^{-4} \text{ eV}^2$  which are intermediate between Cases B1 and B2. In this regime, the mass-squared difference between  $\nu_{1+}$  and  $\nu_{1-}$  is comparable to the MSW intergenerational mass difference, and our approximation scheme is no longer reliable. This region is perhaps best explored numerically, a task beyond the scope of this paper. We have also not explored the implications of the LSND result [40] for Cases B1, B2 and C (it can be trivially accommodated by Case A). Indirect  $\nu_\mu \leftrightarrow \nu_e$  oscillations through an intermediate  $\nu_\tau$  or  $\nu'_\tau$  with an appropriate choice of intergenerational parameters could lead to greater consistency with LSND. (See Ref. [7] for an attempt along these lines in a scenario similar to Case C.) Note that it may not be possible to simultaneously accommodate the LSND result and to produce relic neutrino asymmetry generation [20] such as to ensure consistency with Big Bang Nucleosynthesis in an extension of Cases B1, B2 and C [41]. Case A can accommodate both of these features, but with an energy-independent solar neutrino suppression factor. Cases B1, B2 and C, modified as per the above for greater consistency with LSND, can be made consistent with Big Bang Nucleosynthesis by using a sufficiently large relic neutrino asymmetry that is produced at a high temperature scale by physics unassociated with ordinary–mirror neutrino oscillations (Ref. [42] discusses this type of scenario in more detail).

The Exact Parity Model is, in part, an explicit theory of light, effectively sterile, neutrinos. Its characteristic ordinary–mirror neutrino maximal mixing feature receives strong experimental support from the atmospheric neutrino data. Various possibilities for solving the solar neutrino problem by either averaged vacuum  $\nu_e \leftrightarrow \nu'_e$  oscillations alone (Case A), or several amalgams of MSW-enhanced and vacuum oscillations (Cases B1, B2 and C), exist within the EPM. Future solar neutrino experiments should narrow the possibilities considerably.

## **ACKNOWLEDGMENTS**

This work was supported in part by the Australian Research Council and in part by the Commonwealth of Australia's postgraduate award scheme. YYYW would like to thank John A. L. McIntosh for assistance with preparation of the Figures.

## REFERENCES

- [1] R. Foot, H. Lew and R. R. Volkas, Phys. Lett. **B272**, 67 (1991); see also the concluding section of: T. D. Lee and C. N. Yang, Phys. Rev. **104**, 254 (1956).
- [2] R. Foot and R. R. Volkas, Phys. Rev. **D52**, 6595 (1995); R. Foot, H. Lew and R. R. Volkas, Mod. Phys. Lett. **A7**, 2567 (1992); R. Foot, *ibid.* **A9**, 169 (1994).
- [3] E. Kearns, Talk at *News about SNUS*, ITP Workshop, Santa Barbara, Dec. 1997, available at <http://www.itp.ucsb.edu/online/snu/kearns>.
- [4] R. Foot, R. R. Volkas and O. Yasuda, hep-ph/9801431.
- [5] R. Foot, R. R. Volkas and O. Yasuda, hep-ph/9802287.
- [6] F. Vissani and A. Yu. Smirnov, hep-ph/9710565. See also Ref. [3].
- [7] Q. Y. Liu and A. Yu. Smirnov, hep-ph/9712493.
- [8] Q. Y. Liu, S. P. Mikheyev and A. Yu. Smirnov, hep-ph/9803415; P. Lipari and M. Lusignoli, hep-ph/9803440.
- [9] GALLEX Collaboration, P. Anselmann *et al.*, Phys. Lett. **B285**, 376 (1992); **B285**, 390 (1992); **B314**, 445 (1993); **B327**, 337 (1994); **B357**, 237 (1995); T. Kirsten *et al.* in *Neutrino'96*, Proceedings of the 17th International Conference on Neutrino Physics and Astrophysics, Helsinki, Finland, edited by K. Enqvist, K. Huitu and J. Maalampi (World Scientific, Singapore, 1997), p.3.
- [10] SAGE Collaboration, A. I. Abazov *et al.*, Phys. Rev. Lett. **67**, 3332 (1991); J. N. Abdurashitov *et al.*, Phys. Lett. **B328**, 234 (1994); Phys. Rev. Lett. **77**, 4708 (1996); V. Garvin *et al.* in *Neutrino'96*, Proceedings of the 17th International Conference on Neutrino Physics and Astrophysics, Helsinki, Finland, edited by K. Enqvist, K. Huitu and J. Maalampi (World Scientific, Singapore, 1997), p.14.
- [11] CHOOZ Collaboration, M. Apollonio *et al.*, hep-ex/9711002.
- [12] Kamiokande Collaboration, K.S. Hirata *et al.*, Phys. Rev. Lett. **65**, 1297 (1990); **65**, 1301 (1990); **66**, 9 (1991); Phys. Rev. **D44**, 2241 (1991); Y. Fukada *et al.*, Phys. Rev. Lett. **77**, 1683 (1996).
- [13] R. Svoboda, Talk at *News about SNUS*, ITP Workshop, Santa Barbara, Dec. 1997, available at <http://www.itp.ucsb.edu/online/snu/svoboda>.
- [14] R. Davis, Prog. Part. Nucl. Phys. **32**, 13 (1994); B. T. Cleveland *et al.*, Nucl. Phys. B (Proc. Suppl.) **38**, 47 (1995); K. Lande and P. S. Wildenhain in *Neutrino'96*, Proceedings of the 17th International Conference on Neutrino Physics and Astrophysics, Helsinki, Finland, edited by K. Enqvist, K. Huitu and J. Maalampi (World Scientific, Singapore, 1997), p.25.
- [15] SNO Collaboration, A. B. McDonald in *TAUP'95*, Proceedings of the 4th International Conference on Theoretical and Phenomenological Aspects of Underground Physics, Toledo, Spain, edited by A. Morales, J. Morales and J. A. Villar [Nucl. Phys. **B48** (Proc. Suppl.)], p.357.
- [16] L. Wolfenstein, Phys. Rev. **D17**, 2369 (1978); **D20**, 2634 (1979).
- [17] S. P. Mikheyev and A. Yu. Smirnov, Nuovo Cim. **9C**, 17 (1986).
- [18] For a review on matter effects on neutrino oscillations, see: T. K. Kuo and J. Pantaleone, Rev. Mod. Phys. **61**, 937 (1989).
- [19] P. I. Krastev and S. T. Petcov, Phys. Rev. **D53**, 1665 (1996).
- [20] R. Foot, M. J. Thomson and R. R. Volkas, Phys. Rev. **D53**, 5349 (1996); R. Foot and

R. R. Volkas, *ibid.* **D55**, 5147 (1997); *Astropart. Phys.* **7**, 283 (1997). See also: X. Shi, *Phys. Rev.* **D54**, 2753 (1996).

[21] J. N. Bahcall and M. H. Pinsonneault, *Rev. Mod. Phys.* **67**, 781 (1995).

[22] For the most extreme cases see: A. Dar and G. Shaviv, *Ap. J.* **468**, 933 (1996); K. Fukasaku and T. Fujita, *Prog. Theor. Phys.* **98**, 1251 (1997).

[23] General treatments on oscillating neutrino systems can be found in: S. M. Bilenky and S. T. Petcov, *Rev. Mod. Phys.* **59**, 671 (1987).

[24] S. J. Parke, *Phys. Rev. Lett.* **57**, 1275 (1986).

[25] T. K. Kuo and J. Pantaleone, *Phys. Rev.* **D35**, 3432 (1987).

[26] C. Giunti, C. W. Kim and U. W. Lee, *Phys. Rev.* **D46**, 3034 (1992).

[27] S. M. Bilenky, C. Giunti, C. W. Kim and S. T. Petcov, *Phys. Rev.* **D54**, 4432 (1996).

[28] T. K. Kuo and J. Pantaleone, *Phys. Rev. Lett.* **57**, 1805 (1986).

[29] L. D. Landau, *Phys. Z. Sowjetunion* **2**, 46 (1932); C. Zener, *Proc. Roy. Soc. London, Ser. A* **137**, 696 (1932).

[30] The level-crossing probability is evaluated for an exponential density profile in: S. T. Petcov, *Phys. Lett.* **B200**, 373 (1988).

[31] S. Toshev, *Phys. Lett.* **B185**, 177 (1987); S. T. Petcov and S. Toshev, *ibid* **B187**, 120 (1987); S. T. Petcov, *ibid* **B214**, 259 (1988); P. Langacker *et al.*, *Nucl. Phys.* **B282**, 589 (1987).

[32] A. Baldini and G. F. Giudice, *Phys. Lett.* **B186**, 211, (1987); C. W. Kim, S. Nussinov and W. K. Sze, *ibid* **B184**, 403 (1987).

[33] N. Hata and P. Langacker, *Phys. Rev.* **D56**, 6107 (1997).

[34] G. L. Fogli, E. Lisi and D. Montanino, [hep-ph/9709473](#).

[35] G. L. Fogli, E. Lisi and D. Montanino, [hep-ph/9803309](#).

[36] We have used the standard  $\nu_e \leftrightarrow \nu_{\mu, \tau}$  contours from: G. L. Fogli, E. Lisi and D. Montanino, *Phys. Rev.* **D54**, 2048 (1996).

[37] For standard  $\nu_e \leftrightarrow \nu_{\mu, \tau}$  best fits including Earth regeneration, see: J. N. Bahcall and P. I. Krastev, *Phys. Rev.* **C56**, 2839 (1997); M. Maris and S. T. Petcov, *ibid.* **D56**, 7444 (1997); E. Lisi and D. Montanino, *ibid.* **D56**, 1792 (1997).

[38] See, for example, the  $\nu_e \leftrightarrow \nu_\mu \leftrightarrow \nu_\tau \leftrightarrow \nu_s$  scheme of Ref. [7], the  $\nu_e \leftrightarrow \nu_\mu \leftrightarrow \nu_\tau$  hybrid MSW transition and vacuum oscillation scheme in: Q. Y. Liu and S. T. Petcov, *Phys. Rev.* **D56**, 7392 (1997), etc..

[39] J. Bunn, R. Foot and R. R. Volkas, *Phys. Lett.* **B413**, 109 (1997); R. Foot, R. R. Volkas and O. Yasuda, *Phys. Rev.* **D57**, 1345 (1998).

[40] LSND Collaboration, C. Athanassopoulos *et al.*, *Phys. Rev. Lett.* **77**, 3082 (1996); [nucl-ex/9706006](#); [nucl-ex/9709006](#).

[41] We thank R. Foot for emphasising this point to us.

[42] R. Foot and R. R. Volkas, *Phys. Rev. Lett.* **75**, 4350 (1995).

## TABLES

TABLE I. Solar neutrino measurements and theoretical expectations within the standard solar model of Bahcall and Pinsonneault (SSM-BP) (1995) [21]. Capture rates for Homestake [14], GALLEX [9] and SAGE [10] are given in SNU, where  $1 \text{ SNU} = 10^{-36}$  capture per atom per second. For Kamiokande [12] and SuperKamiokande [13], the measured neutrino flux is given in  $10^6 \text{ cm}^{-2} \text{ s}^{-1}$ . The associated statistical and systematic errors ( $1\sigma$ ) are quoted for each experiment.

Experiment	Measurement	SSM-BP
Homestake	$2.56 \pm 0.16 \pm 0.14$	$9.3^{+1.2}_{-1.4}$
GALLEX	$69.7 \pm 6.7^{+3.9}_{-4.5}$	$137^{+8}_{-7}$
SAGE	$72^{+12+5}_{-10-7}$	$137^{+8}_{-7}$
Kamiokande	$2.80 \pm 0.19 \pm 0.33$	$6.62^{+0.93}_{-1.12}$
SuperKamiokande	$2.51^{+0.14}_{-0.13} \pm 0.18$	$6.62^{+0.93}_{-1.12}$

TABLE II. The mixing angle  $\eta$ , the effective density  $A_{eff}$  and the off-diagonal matter-induced mixing term  $A_{ind}$  evaluated for various combinations of  $\nu_{1h}$  and  $\nu_{2\ell}$  for Case B1.

$\nu_{1h} \leftrightarrow \nu_{2\ell}$	$\sin \eta$	$A_{eff}$	$A_{ind}$
$\nu_{1-} \leftrightarrow \nu_{2-}$	$\sin \phi$	$\frac{A_{CC}}{2}$	0
$\nu_{1-} \leftrightarrow \nu_{2+}$	$\frac{\sin \theta}{\sqrt{\cos^2 \phi + \sin^2 \theta}}$	$\frac{A_{CC}}{2} (\cos^2 \phi + \sin^2 \theta) + A_{NC} \sin 2\eta \sin(\theta - \phi)$	$A_{NC} \cos 2\eta \sin(\theta - \phi)$
$\nu_{1+} \leftrightarrow \nu_{2+}$	$\sin \theta$	$\frac{A_{CC}}{2}$	0
$\nu_{1+} \leftrightarrow \nu_{2-}$	$\frac{\sin \phi}{\sqrt{\cos^2 \theta + \sin^2 \phi}}$	$\frac{A_{CC}}{2} (\cos^2 \theta + \sin^2 \phi) - A_{NC} \sin 2\eta \sin(\theta - \phi)$	$-A_{NC} \cos 2\eta \sin(\theta - \phi)$

TABLE III. The mixing angles  $\psi$  and  $\eta$ , the effective density  $A_{eff}$  and the off-diagonal matter-induced mixing term  $A_{ind}$  evaluated for various combinations of  $\nu_{1\ell}$ ,  $\nu_{1h}$  and  $\nu_{2\ell}$  for Case B2.

$\nu_{1\ell} \leftrightarrow \nu_{2\ell}$	$\sin \psi$	$\sin \eta$	$A_{eff}$	$A_{ind}$
$\nu_{1h}$				
$\nu_{1+} \leftrightarrow \nu_{2-}$	$\frac{\cos \phi}{\sqrt{\cos^2 \theta + \cos^2 \phi}}$	$\frac{\sin \phi}{\sqrt{1 + \cos^2 \theta}}$	$\frac{A_{CC}}{2} (1 + \cos^2 \theta) + \frac{A_{NC}}{2} [\cos 2\eta \sin 2\psi \cos(\theta - \phi) - 2 \sin 2\eta \cos \psi \sin(\theta - \phi)]$	$-A_{NC} [\cos 2\eta \cos \psi \sin(\theta - \phi) + \frac{1}{2} \sin 2\eta \sin 2\psi \cos(\theta - \phi)]$
$\nu_{1-} \leftrightarrow \nu_{2-}$	$\frac{\cos \theta}{\sqrt{\cos^2 \theta + \cos^2 \phi}}$	$\frac{\sin \phi}{\sqrt{1 + \cos^2 \theta}}$	$\frac{A_{CC}}{2} (1 + \cos^2 \theta) + \frac{A_{NC}}{2} [\cos 2\eta \sin 2\psi \cos(\theta - \phi) - 2 \sin 2\eta \sin \psi \sin(\theta - \phi)]$	$-A_{NC} [\cos 2\eta \sin \psi \sin(\theta - \phi) + \frac{1}{2} \sin 2\eta \sin 2\psi \cos(\theta - \phi)]$
$\nu_{1-} \leftrightarrow \nu_{2+}$	$\frac{\cos \theta}{\sqrt{\cos^2 \theta + \cos^2 \phi}}$	$\frac{\sin \theta}{\sqrt{1 + \cos^2 \phi}}$	$\frac{A_{CC}}{2} (1 + \cos^2 \phi) + \frac{A_{NC}}{2} [\cos 2\eta \sin 2\psi \cos(\theta - \phi) + 2 \sin 2\eta \cos \psi \sin(\theta - \phi)]$	$A_{NC} [\cos 2\eta \cos \psi \sin(\theta - \phi) - \frac{1}{2} \sin 2\eta \sin 2\psi \cos(\theta - \phi)]$
$\nu_{1+} \leftrightarrow \nu_{2+}$	$\frac{\cos \phi}{\sqrt{\cos^2 \theta + \cos^2 \phi}}$	$\frac{\sin \theta}{\sqrt{1 + \cos^2 \phi}}$	$\frac{A_{CC}}{2} (1 + \cos^2 \phi) + \frac{A_{NC}}{2} [\cos 2\eta \sin 2\psi \cos(\theta - \phi) + 2 \sin 2\eta \sin \psi \sin(\theta - \phi)]$	$A_{NC} [\cos 2\eta \sin \psi \sin(\theta - \phi) - \frac{1}{2} \sin 2\eta \sin 2\psi \cos(\theta - \phi)]$

TABLE IV. The allowed intergenerational oscillation parameters  $\Delta m^2$  and  $\sin^2 2\eta$  for Cases B1, B2 and C. The best fit oscillation parameters in the small mixing angle (SMA) and the large mixing angle (LMA) solutions for standard  $2\nu$  scenarios [33,37] are also included.

Scheme	$\Delta m^2/eV^2$	$\sin^2 2\eta$
Standard $\nu_e \leftrightarrow \nu_{\mu, \tau}$ SMA	$5 \times 10^{-6}$	$8 \times 10^{-3}$
Standard $\nu_e \leftrightarrow \nu_{\mu, \tau}$ LMA	$1.6 \times 10^{-5}$	0.63
Standard $\nu_e \leftrightarrow \nu_s$ SMA	$4 \times 10^{-6}$	$10^{-2}$
Case B1	$2 \times 10^{-6} \rightarrow 5 \times 10^{-5}$	$8 \times 10^{-4} \rightarrow 0.1$
Case B2	$10^{-5} \rightarrow 10^{-4}$	$10^{-4} \rightarrow 4 \times 10^{-3}$
Case C	$4 \times 10^{-6} \rightarrow 5 \times 10^{-6}$	$8 \times 10^{-3} \rightarrow 10^{-2}$

TABLE V. Predictions for future experiments. The amount of Boron spectral distortion associated with each case is qualitatively compared with the standard  $2\nu$  predictions (maximal for SMA and minimal for LMA). The approximate Beryllium fluxes to be measured by BOREXINO prescribed by our various cases relative to the no-oscillation flux are also compared. The last column shows the predicted ranges of the ratio of charged to neutral current event rate relative to the no-oscillation rate at SNO.

Scheme	Boron spectral distortion	Be flux ( $\frac{\text{predicted}}{\text{SSM}}$ )	$r_d$ for SNO
Standard $\nu_e \leftrightarrow \nu_{\mu, \tau}$ SMA	maximal	$\sim 0$	$0.25 \rightarrow 0.4$
Standard $\nu_e \leftrightarrow \nu_{\mu, \tau}$ LMA	minimal	$\sim 0.4$	$\sim 0.2$
Standard $\nu_e \leftrightarrow \nu_s$ SMA	maximal	$\sim 0$	1
Case A	none	$\frac{1}{2}$	1
Case B1	intermediate	$\frac{1}{4} \rightarrow \frac{1}{2}$	$0.5 \rightarrow 0.75$
Case B2	intermediate	$\sim \frac{1}{2}$	$0.4 \rightarrow 0.7$
Case C	maximal	$\sim 0$	$0.45 \rightarrow 0.6$

## FIGURES

FIG. 1. Level-crossing diagram for Case B1. The labels  $\nu_i^m$ , where  $i = 1\ell, 1h, 2\ell, 2h$ , denote the instantaneous mass eigenstates. The letter  $R$  labels the intergenerational MSW resonance.

FIG. 2. The  $\nu_e$  survival probability at the Earth for Case B1 with  $\Delta m_{21}^2 = 5 \times 10^{-6} eV^2$  and  $\sin^2 2\eta = 8 \times 10^{-3}$  (solid line) for  $\nu_e$  produced at the centre of the sun. The dashed and dotted lines represent, respectively, the survival probabilities for the standard  $\nu_e \leftrightarrow \nu_{\mu,\tau}$  and  $\nu_e \leftrightarrow \nu_s$  scenarios evaluated for the same oscillation parameters.

FIG. 3. Level-crossing diagram for Case B2. The labels  $\nu_i^m$ , where  $i = 1\ell, 1h, 2\ell, 2h$ , denote the instantaneous mass eigenstates. Two resonances are identified and labelled as  $R_L$  and  $R_H$ , where  $R_H$  is the resonance of interest.

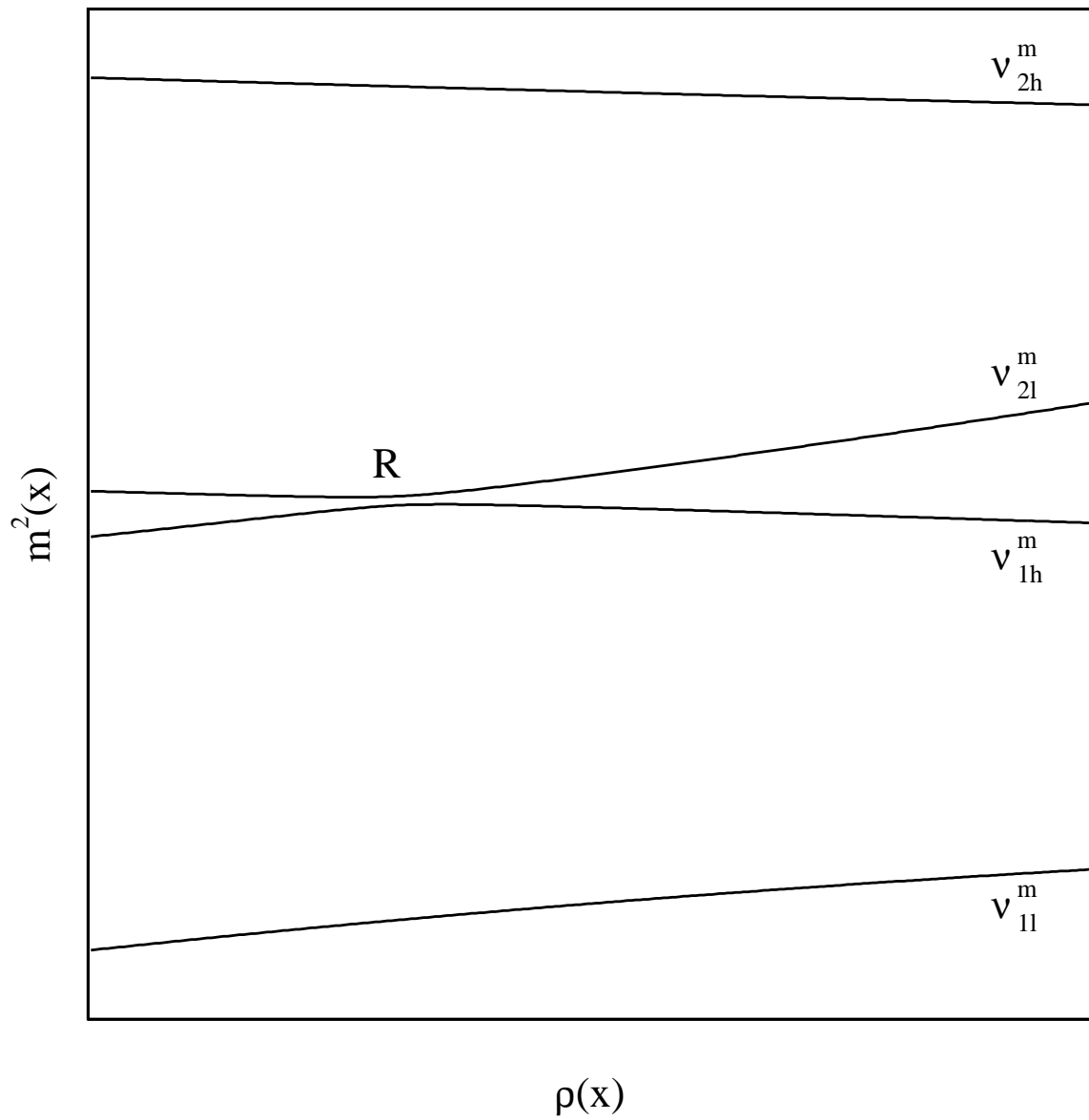
FIG. 4. The  $\nu_e$  survival probability at the Earth for Case B2 with  $\Delta m_{21}^2 = 5 \times 10^{-6} eV^2$  and  $\sin^2 2\eta = 8 \times 10^{-3}$  (solid line) for  $\nu_e$  produced at the centre of the sun. The dashed and dotted lines represent, respectively, the survival probabilities for the standard  $\nu_e \leftrightarrow \nu_{\mu,\tau}$  and  $\nu_e \leftrightarrow \nu_s$  scenarios evaluated for the same oscillation parameters.

FIG. 5. The  $\nu_e$  survival probability at the Earth for Case C with  $\Delta m_{21}^2 = 5 \times 10^{-6} eV^2$  and  $\sin^2 2\eta = 8 \times 10^{-3}$  (solid line) for  $\nu_e$  produced at the centre of the sun. The dashed and dotted lines represent, respectively, the survival probabilities for the standard  $\nu_e \leftrightarrow \nu_{\mu,\tau}$  and  $\nu_e \leftrightarrow \nu_s$  scenarios evaluated for the same oscillation parameters.

FIG. 6. The approximate allowed regions for Cases B1 (area enclosed by the dot-dash line) and B2 (area enclosed by the dashed line). These correspond to the regions in which the  $2\sigma$  bands (including theoretical uncertainties) of all five solar neutrino experiments (see Table I) overlap, respectively for Cases B1 and B2. Note that these regions will differ slightly from those generated from a  $\chi^2$ -analysis. The allowed region for the standard  $2\nu$  case at 95% C.L. (dotted line) is shown here for the purpose of comparison [33]. The solution to Case C is similar to this.

FIG. 7. The  $\nu_e$  survival probability at the Earth for Case B1 evaluated for various  $\Delta m_{21}^2$  and  $\sin^2 2\eta$  shown on the graphs (solid line) for  $\nu_e$  produced at the centre of the sun. These parameters lie within the allowed region for Case B1 but are not necessarily the best fit parameters. For the purpose of comparison, the survival probabilities for the standard  $\nu_e \leftrightarrow \nu_{\mu,\tau}$  small angle solution (dashed line) and large angle solution (dotted line) (see Table IV for the best fit parameters) are also shown.

FIG. 8. The  $\nu_e$  survival probability at the Earth for Case B2 evaluated for various  $\Delta m_{21}^2$  and  $\sin^2 2\eta$  shown on the graphs (solid line) for  $\nu_e$  produced at the centre of the sun. These parameters lie within the allowed region for Case B2 but are not necessarily the best fit parameters. For the purpose of comparison, the survival probabilities for the standard  $\nu_e \leftrightarrow \nu_{\mu,\tau}$  small angle solution (dashed line) and large angle solution (dotted line) (see Table IV for the best fit parameters) are also shown.



$$\rho(x)$$

FIG. 1

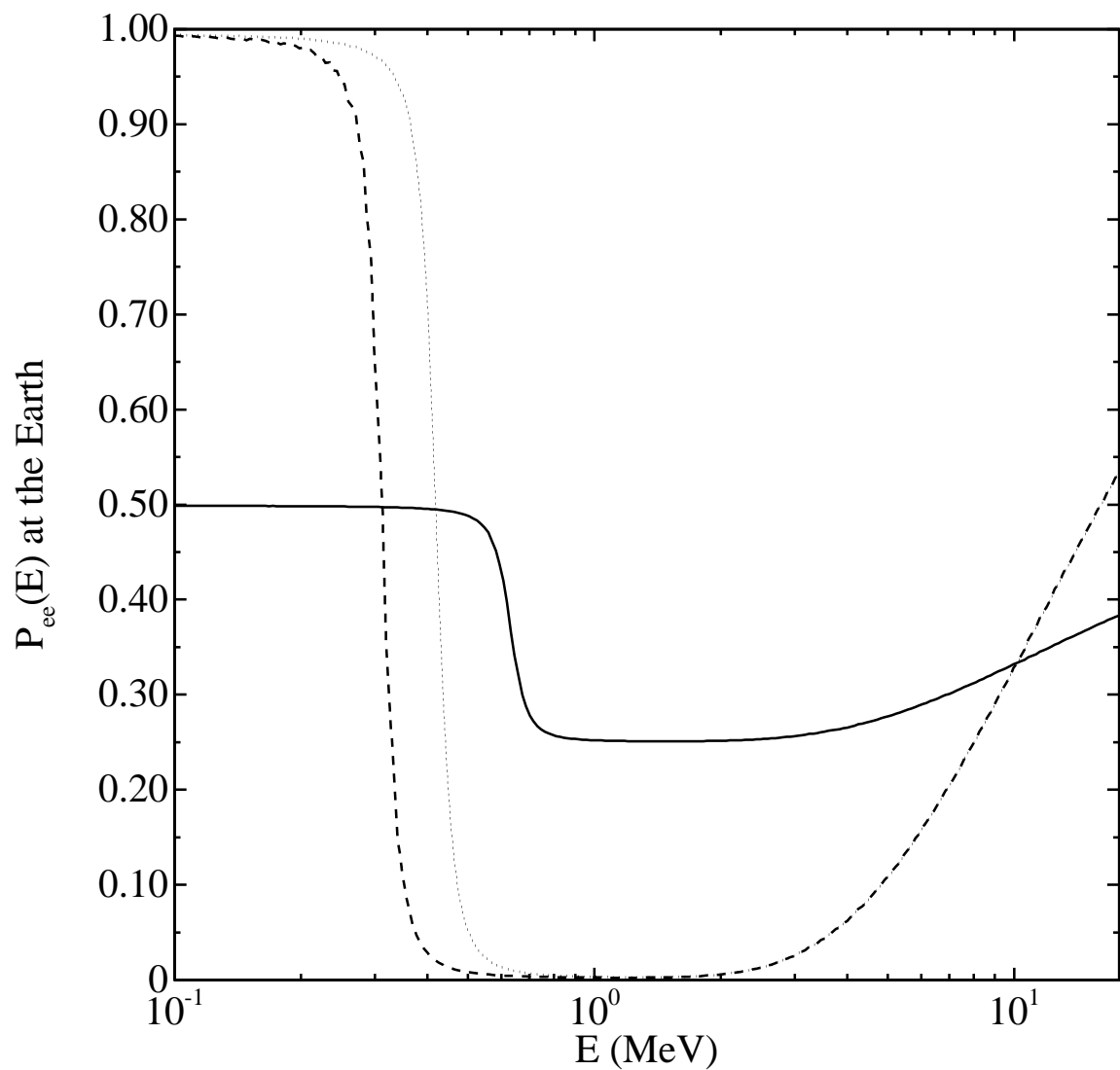


FIG. 2

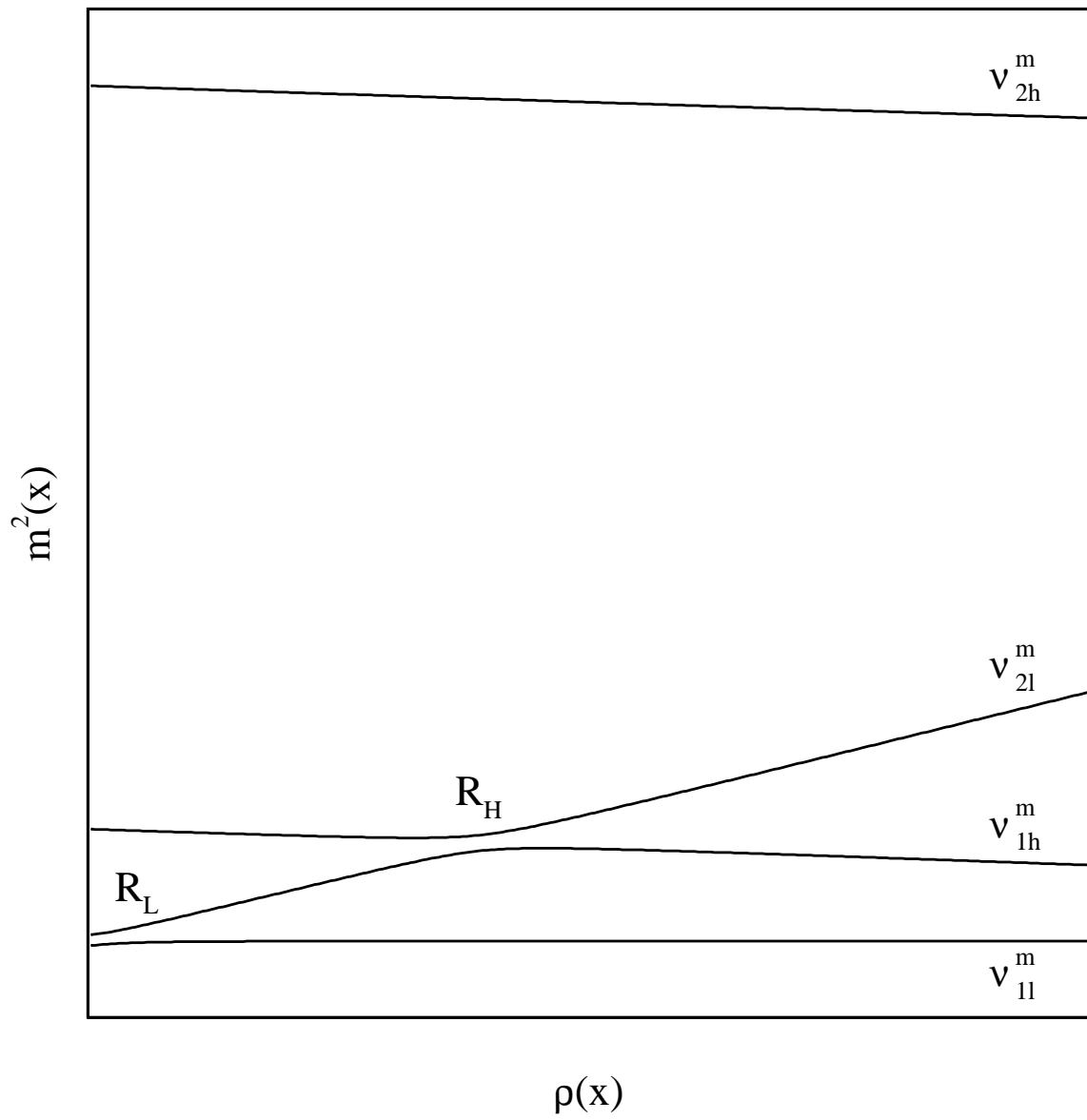


FIG. 3

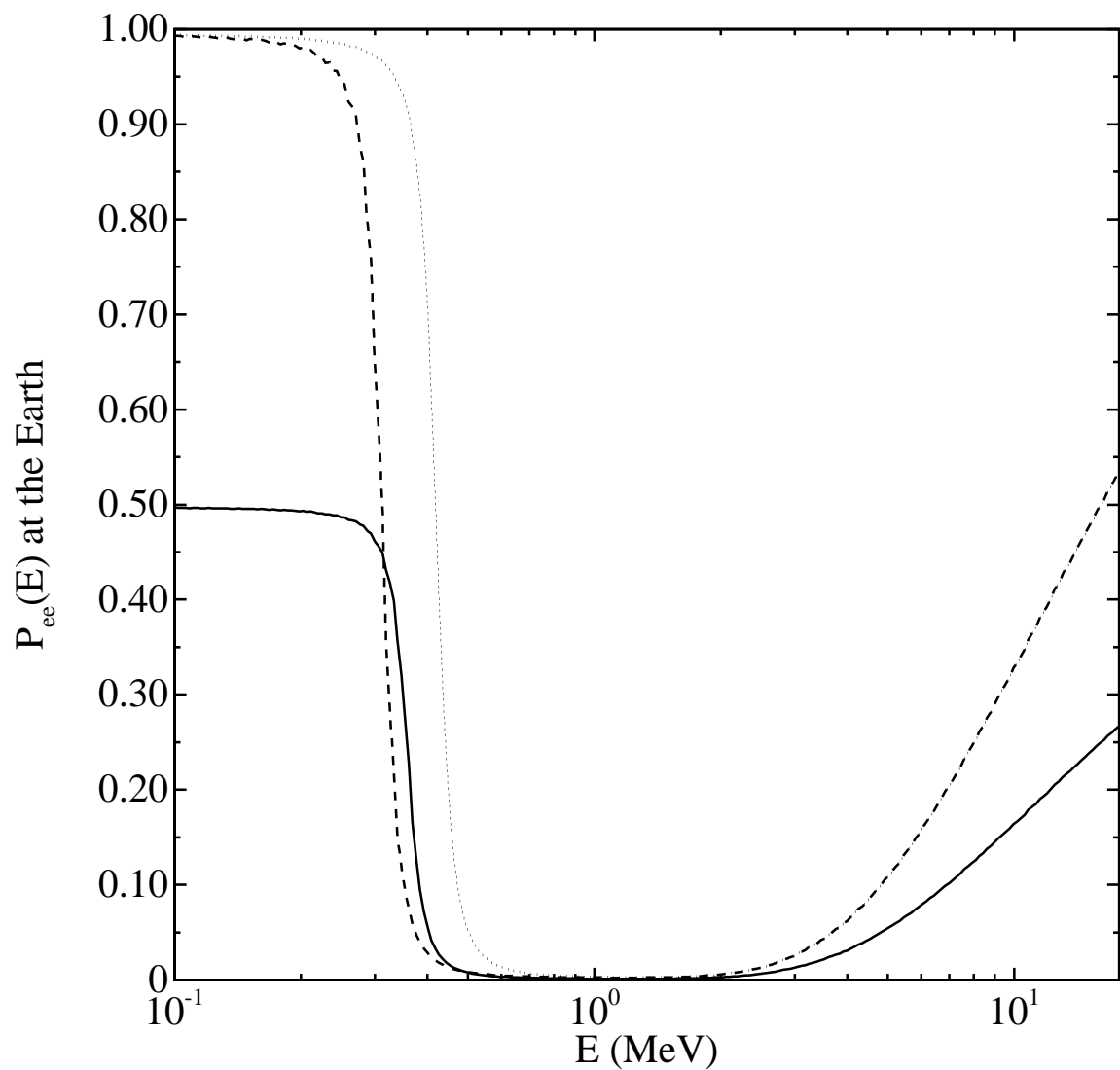


FIG. 4

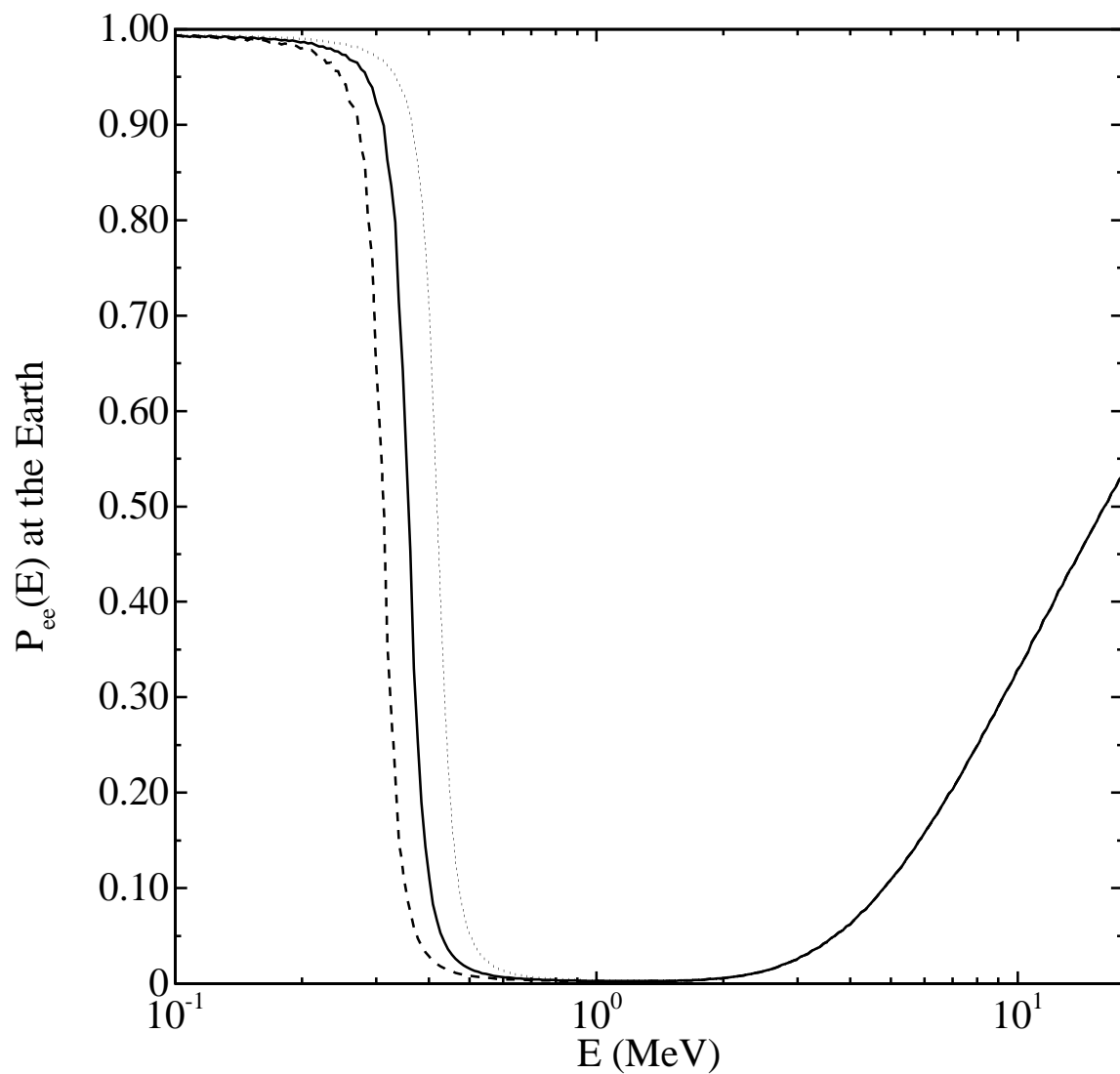


FIG. 5

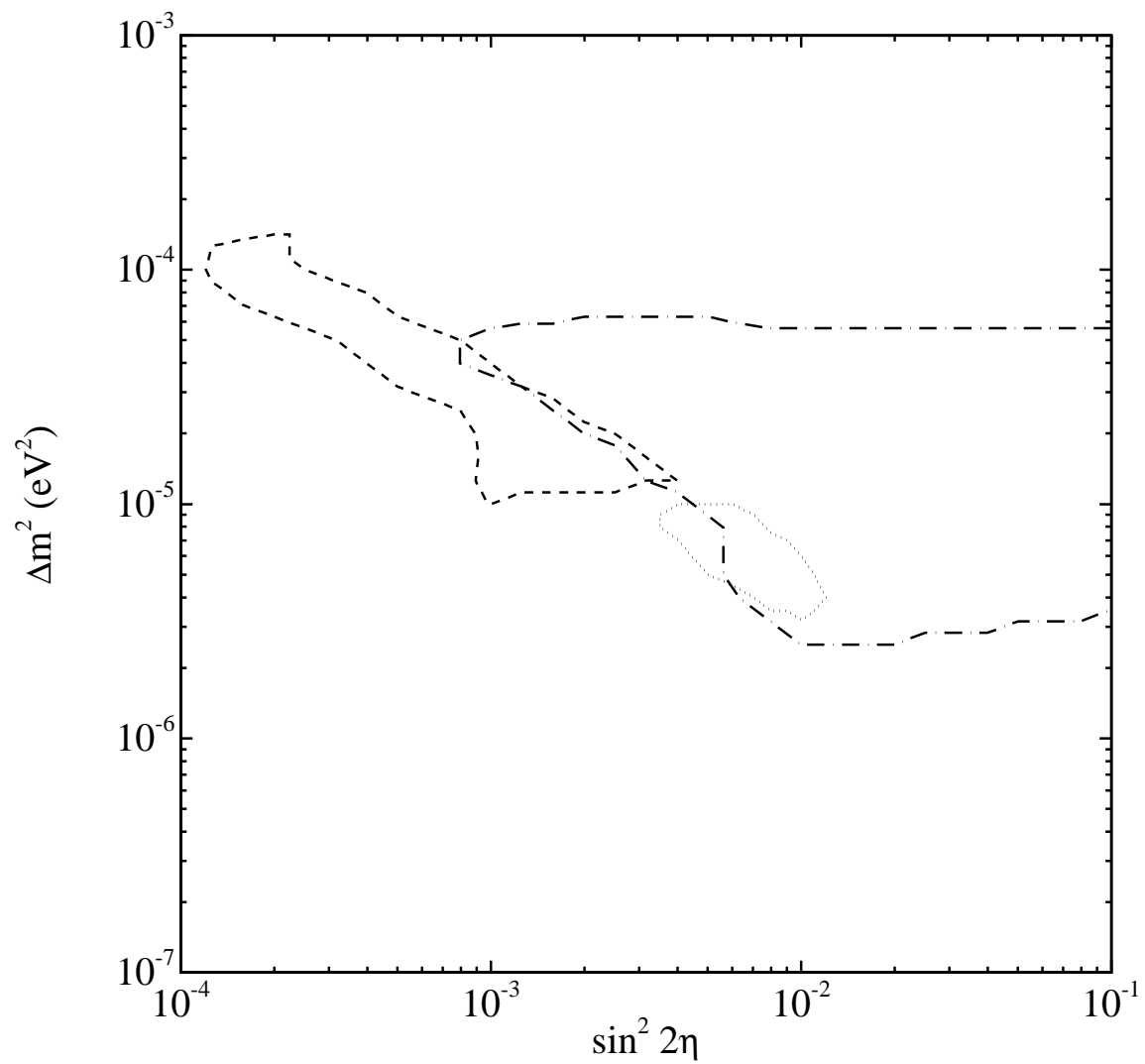


FIG. 6

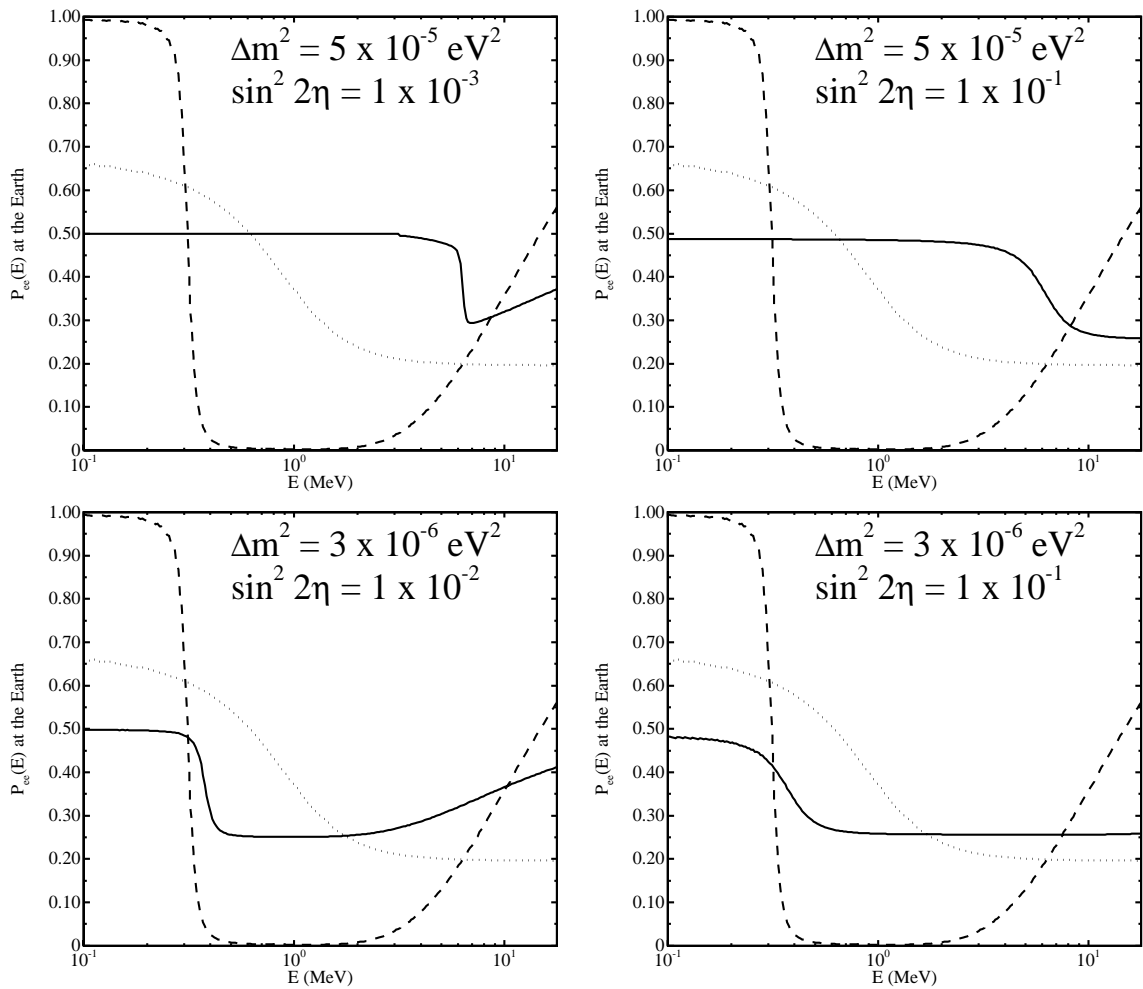


FIG. 7

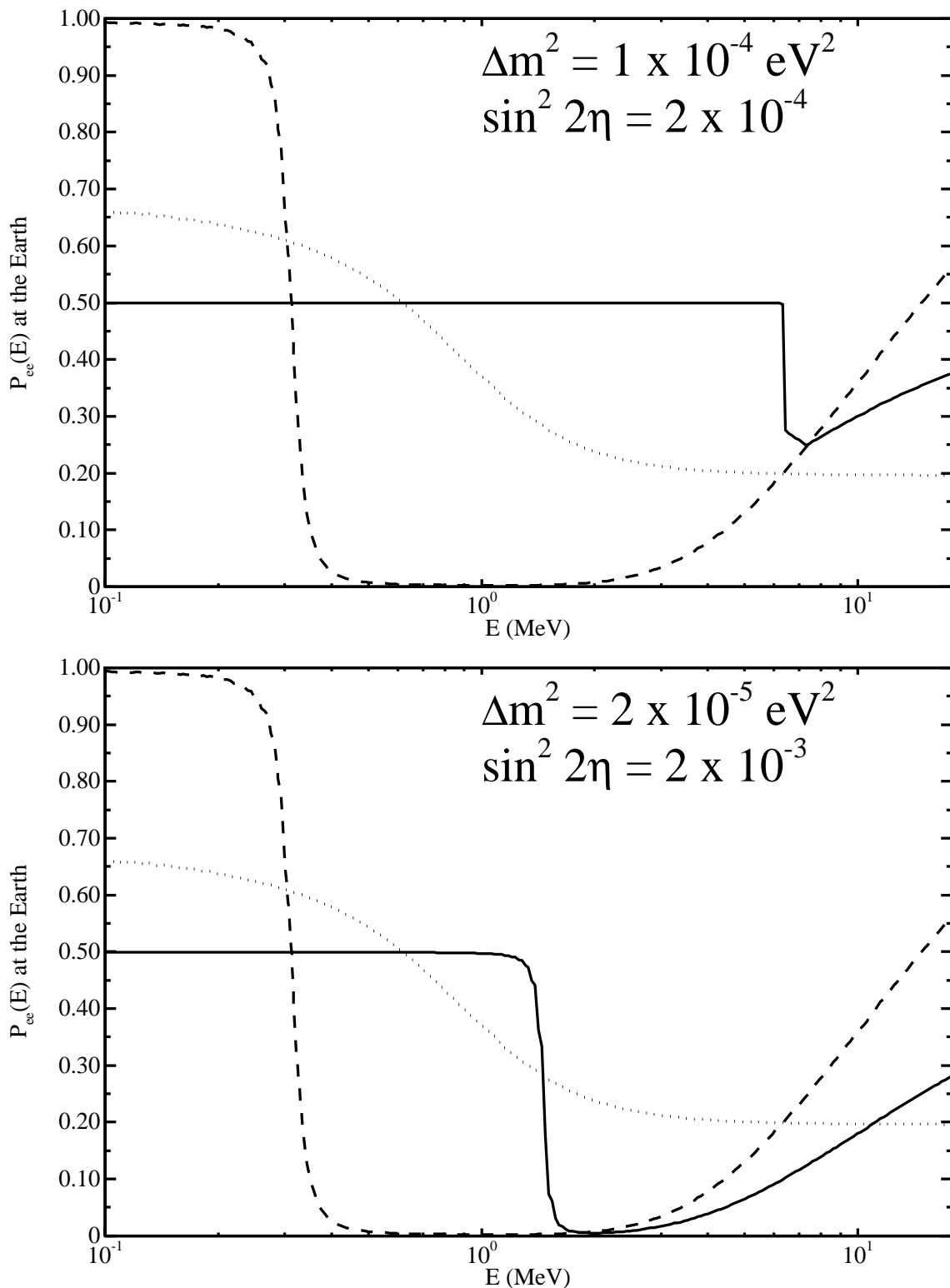


FIG. 8